Applied Energy 279 (2020) 115853

Contents lists available at ScienceDirect

Applied Energy

journal homepage: www.elsevier.com/locate/apenergy

Feasibility study of a blind-type photovoltaic roof-shade system designed for simultaneous production of crops and electricity in a greenhouse

Zhi Li [a,b], Akira Yano [a,*], Hidekazu Yoshioka [a]

[a] Institute of Environmental Systems Science, Shimane University, 1060 Nishikawatsu, Matsue, Shimane 690-8504, Japan
[b] The United Graduate School of Agricultural Sciences, Tottori University, 4-101 Koyama-Minami, Tottori 680-8553, Japan

HIGHLIGHTS

- Renewable energy use in modern greenhouse management is crucially important.
- A unique semi-transparent photovoltaic (PV)-blind system was examined numerically.
- The PV blind rotated automatically in response to sunlight variation.
- The PV blind can meet greenhouse electrical energy demands.
- Crops below the PV blind roof can be irradiated sufficiently by solar energy.

GRAPHICAL ABSTRACT

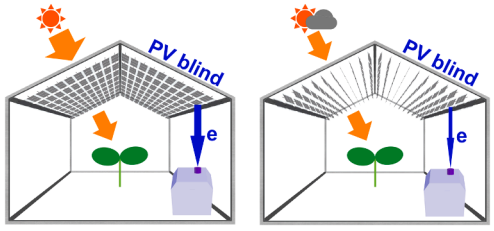

ARTICLE INFO

Keywords:
Food
Renewable energy
Shading
Solar cell
Sustainability

ABSTRACT

The use of renewable energy in modern greenhouse management is important to achieve efficient and sustainable food supplies for a world with increasing population. This study assessed the performance of a blind-type shading regulator that can automatically rotate semi-transparent photovoltaic (PV) blades installed on the greenhouse roof in response to sunlight variation. The PV blind oriented parallel to the roof partially blocked intense sunlight penetration into the greenhouse, but it transmitted sunlight during cloudy time by turning the blind bearing to be perpendicular to the roof. A stable irradiation environment is therefore producible in the greenhouse under variable sky conditions. Annual operations demonstrated that the blinds' own generated electrical energy can sustain PV blind operation and produce surplus electrical energy. The PV blind electricity generation and sunlight availability for crops below the PV blind roof were calculated based on a mathematical model developed using theoretical sunlight parameters and the experimentally obtained PV blind system parameters. Assuming cloudless skies and threshold irradiance for blind rotation set at 500 W m^{-2}, 13.0 and 12.3 kWh m^{-2} yr^{-1} surplus electrical energy can be generated, respectively, by north–south and east–west oriented model greenhouses. Cloudy skies reduce surplus electrical energy production by 50%, but PV blinds can supply greenhouse electrical energy demands partially or completely, depending on the degree of greenhouse electrification. Below the PV blinds, 8–10 MJ m^{-2} day^{-1} of insolation is expected to irradiate crops under actual sky conditions. This insolation is sufficient to cultivate major horticultural crops. Regulating the threshold irradiance level for PV blind turning can control the sunlight apportionment ratio for cultivation and electricity generation, thereby enabling sustainable energy–food dual production in a greenhouse.

* Corresponding author.
E-mail address: yano@life.shimane-u.ac.jp (A. Yano).

https://doi.org/10.1016/j.apenergy.2020.115853
Received 9 June 2020; Received in revised form 21 August 2020; Accepted 5 September 2020
Available online 19 September 2020

Nomenclature

A_{PV}	PV module azimuth (rad)
A_S	solar azimuth (rad)
dt	infinitesimal time interval (s)
de_{charge}	energy charged into the battery during dt (J)
$E_{circuit}$	energy consumption at the motor control circuit (kWh)
E_{motor}	energy consumed by the DC motor (kWh)
E_{loss}	system energy loss (kWh)
E_{PV}	PV generated energy (kWh)
$E_{surplus}$	surplus electrical energy (kWh)
e	the equation of time (min)
h	solar altitude (rad)
I_{back}	global irradiance on the PV blind back-surface (W m^{-2})
$I_{back\ diffuse}$	diffuse irradiance received by the PV blind back-surface (W m^{-2})
$I_{back\ direct}$	direct irradiance received by the PV blind back-surface (W m^{-2})
$I_{back\ reflect}$	ground reflected irradiance received by the PV blind back-surface (W m^{-2})
I_{crop}	global irradiance received by crops positioned at the model greenhouse center (W m^{-2})
$I_{crop\ diffuse}$	diffuse irradiance received by crops positioned at the model greenhouse center (W m^{-2})
$I_{crop\ direct}$	direct irradiance received by crops positioned at the model greenhouse center (W m^{-2})
$I_{diffuse}$	diffuse irradiance on a horizontal surface (W m^{-2})
I_{direct}	direct irradiance on a horizontal surface (W m^{-2})
I_{front}	global irradiance on the PV blind front-surface (W m^{-2})
$I_{front\ diffuse}$	diffuse irradiance received by the PV blind front-surface (W m^{-2})
$I_{front\ direct}$	direct irradiance received by the PV blind front-surface (W m^{-2})
$I_{front\ reflect}$	ground reflected irradiance received by the PV blind front-surface (W m^{-2})
I_H	horizontal global irradiance (W m^{-2})
$I_{threshold}$	threshold I_H for PV blind rotation (W m^{-2})
I_0	solar constant, 1.37×10^3 (W m^{-2})
i_{charge}	battery charge current (A)
i_{load}	load current (A)
i_{PV}	single PV generated current (A)
i_{3PV}	triple PV generated current (A)
J_{back}	insolation originated from I_{back} (MJ m^{-2})
J_{crop}	insolation onto crops cultivated at the model greenhouse floor center (MJ m^{-2})
J_{front}	insolation originated from I_{front} (MJ m^{-2})
$J_{front} + J_{back}$	insolation received by the bifacial PV blinds (MJ m^{-2})
J_H	global horizontal insolation (MJ m^{-2})
k	number of charge–discharge controllers
l	number of motor control circuits
M	the set of measurement times t when $h_t > 0$ with 10 s intervals from 8 December 2017 through 7 December 2018
m	number of DC motors
n	number of PV modules
P_{charge}	battery power (W)
$P_{circuit}$	control circuit power (W)
P_{load}	power supplied to the load (W)
P_{loss}	system power loss (W)
P_{motor}	power supplied to the DC motor (W)
P_{max}	the peak value of each P_{PV} curve of the single PV module (W)
P_{PV}	generated power of the single PV module (W)
P_{3PV}	generated power of the triple PV modules (W)
p	atmospheric transmissivity
S_{PV}	single PV module area (m^2)
T	number of days elapsed from 1 January (day)
TST	true solar time (hour)
t	time beginning at 00:00:00, 1 January (s)
V_{charge}	battery voltage (V)
$V_{discharge}$	voltage at the charge–discharge controller load terminal (V)
V_{PV}	voltage of the single PV module (V)
V_{3PV}	voltage of the triple PV modules (V)
β	PV blind inclination (rad)
γ_{front}	angle between direct beam sunlight and the PV blind front-normal (rad or degree)
γ_{back}	angle between direct beam sunlight and the PV blind back-normal (rad or degree)
δ	solar declination (rad)
ε	the transmittance coefficient of greenhouse glass (%)
η_M	PV module efficiency (%)
θ	angle between the PV blind surface and the greenhouse roof surface (degree); $\theta = 0^\circ$ when the PV blinds are parallel to the greenhouse roof surface.
κ	conversion coefficient from calculated P_{max} to P_{PV}
μ	the ratio of measured I'_H to calculated I_H
ρ	ground albedo
φ	latitude (degree)
ψ	longitude (degree)
ω	hour angle (rad)

As described in this paper, most variables depend on time t. Subscript "$_t$" is added to the mathematical symbols when necessary. For example, "$I_{H,t}$" represents the calculated horizontal global irradiance at t. Relevant experimentally measured data are also presented. To distinguish the calculated and measured values of the same quantity, the "prime" is added for the measured values. For example, "I'_H" represents the measured horizontal global irradiance.

1. Introduction

The world is confronting population growth and global warming. Enhancement and diversification of food production and the development of renewable energy systems to diminish dependence on fossil fuels are therefore urgent issues [1,2]. Greenhouse cultivation is a major supplier of green vegetables and fruits in the agricultural sector. Recently, protected agricultural areas including greenhouses, low tunnels, and net houses exceeded 5 million hectares [3]. Greenhouse cultivation presents remarkable benefits such as 1) crop production in seasons and regions that are unsuitable for field cultivation, 2) physical blockage of insect invasions, and 3) minimized water and fertilizer consumption [4]. Nevertheless, fuel and electric power are necessary to manage greenhouse environments and maintain suitable cultivation conditions [5,6]. Modern greenhouse cultivation is therefore a major fossil fuel consumer as well as a major CO_2 emitter in the horticultural sector [1,7]. Reduction of energy demand and utilization of renewable energy for greenhouse environmental control are therefore important to overcome the myriad of challenging issues [8].

Photovoltaic (PV) power generation has spread around the world from small-scale embedded systems in electronic devices to large-scale arrays deployed across fields of many hectares [9,10]. Sunlight is fundamentally necessary to generate electrical power using PVs. Moreover, the main prerequisite of cultivation is sunlight availability to crops because crop growth depends entirely on photosynthesis. Those sunlight requirements for crops and PVs are mutually exclusive to the degree that, until the end of the 20th century, few scholarly reports described studies related to sharing of greenhouse spaces for crop cultivation and PV electricity generation [11]. Recently, the coexistence of PV power generation and greenhouse cultivation has been actively studied, particularly in high insolation regions where cultivation has been conducted under deliberate shading conditions [12]. The use of PVs as a sunshade material can be beneficial under such circumstances [2]. Although the greatest amount of electrical energy is producible with full cover of a greenhouse roof by PVs, the interior sunlight can become too weak to grow crops [13,14,15]. In other cases, the greenhouse can be too hot to grow crops in summer without shading [16,17]. Therefore, some appropriate shading level can be expected to exist somewhere in between. Consequently, several studies have explored an acceptable roof coverage rate by PVs. In Italy, high-quality wild rocket was produced in a greenhouse on which PV modules covered 32% of the roof area in a striped arrangement [18]. Berry cultivated under the 32% PV roof cover exhibited increased total anthocyanins, total phenols, and antioxidant capacity [19]. Tomato production tests conducted under PV greenhouse roofs in southern Europe and Africa demonstrated that 10% roof area coverage by checkerboard-patterned PVs does not affect yield [20,21,22], although 15, 30, and 50% roof coverage ratios were found to reduce yields [13,14,17,23]. Increased fruit production of peppers

cultivated in a Greek greenhouse, the roof of which was covered by 20% with opaque PV modules, has been reported [24]. In Kunming, China, superior strawberry growth, quality, and yield were reported for in a greenhouse with 26% roof area PV coverage [25].

Although those partial PV roof covers are effective on sunny days, shading becomes excessive for cultivation during cloudy or low-irradiance periods. Removing PVs or changing PV bearings in response to solar irradiance variation are some possible solutions. The mode of adjusting the shading level by rotating the roof-integrated PV modules, similar to venetian blind operation, has been proposed by Vadiee et al. [26,27,28], Marucci et al. [16,29,30,31], and Li et al. [32,33]. Unlike sun-tracking systems, which prioritize electricity production [34], the blind type systems let moderate sunlight pass through the roof to crops below the PV panels. Although each early PV-blind study has opened up new possibilities for the coexistence of crop cultivation and PV power generation, efforts toward practical realization are still underway.

For this study, we pursued the prospect of deploying PV blinds prototyped by Li et al. [32,33]. Semi-transparent PVs were used as the blind blades. They were directed parallel to the greenhouse roof surface with a moderate shading rate and increased power generation when solar irradiance was higher than a predetermined threshold level. When irradiance was less than the threshold level, the PV blinds were turned perpendicular to the greenhouse roof surface to prioritize sunlight intake to the greenhouse crops, although the PV power generation was thereby sacrificed. Accordingly, the sunlight level on the crops below the PV blind can be controlled in an adequate range. The PV blind system assisted with a battery energy storage realized a stand-alone power system to cover the energy demand for the automatic PV blind operations in response to solar irradiance variation. Mathematical models are a useful means to analyze the performance of the PV blind system for achieving an improved greenhouse shading control under stochastic sky conditions [35]. Using parameters obtained from the empirical experiments, we established a mathematical model to calculate the electrical energy budget of the PV blind system and to calculate the insolation utilization balance between cultivation and electricity generation.

This study contributes to the body of knowledge related to renewable energy applications in the greenhouse industries [36,37] by introducing the novel dynamic control of the PV blind system. The PV blind aims at crop–energy dual production at an optimum balance between the two products to sustain both agricultural and PV activities on a parcel of arable land. Crop-level solar irradiance is sometimes too weak to drive optimal photosynthesis, whereas it is sometimes excessive. Nevertheless, PV systems introduced for use at agricultural sites to date have not possessed any automatic controllability of the shading rate on crops cultivated below the PVs [38,39]. This deficiency often caused crop yield loss [40]. The novel PV blinds automatically turn when the sunlight is weak, leaving gaps between the PV panels to maximize the sunlight reaching the crops at the expense of power generation. As the result, a normal crop yield is assured. This paper also presents a newly developed algorithm for designing the energy balance between the PV electricity generation and available insolation for crops below the PVs. By controlling the blind orientation based on the mathematical model, farmers can set the balance between the crop production and electricity generation, strategically. In addition to their angle controllability, the unique semi-transparency of the PV blinds augments the dual-use opportunity of sunlight. Applications of semi-transparent PV cells of various types have been studied for residential window glazing [41,42] and blinds [43,44]. Unlike human dwelling, which have windows installed in some walls, entire roof areas and walls of greenhouses are transparent glazing. Accordingly, greenhouses present greater opportunities of semi-transparent PV applications. The modest shading alleviates thermal damage to plants when solar irradiance is excessive. These concepts prioritize the fundamental role of greenhouses as a crop production facility. This paper presents a clue of bridging the current gap existing between PV developers who need space to increase the renewable energy proportion among the global energy supply and farmers who challenge to improve crop production efficiency on limited arable land to feed increasing population.

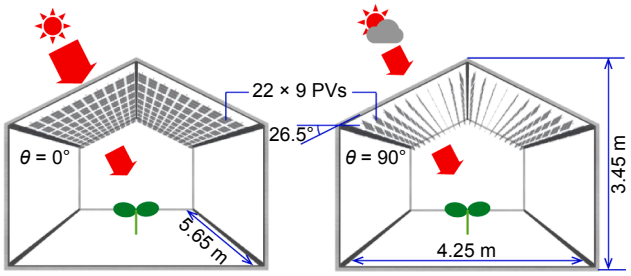

Fig. 1. Model greenhouse equipped with PV blinds at closed ($\theta = 0°$) and open ($\theta = 90°$) orientations according to the degree of irradiance. Underneath the greenhouse glass roof, 198 PV modules can be installed neatly.

The composition of this paper is the following. Section 2 represents the model greenhouse designed to analyze the prototype PV blind system performance. The system configuration and the sunlight and PV module parameters are defined. Then the electrical characteristics of the PV blind with respect to the direct sunlight angles are reported in Section 3. Using experimentally obtained data, the electrical energy balance equation of the prototype system is described in Section 4. Based on the established mathematical model, we evaluated the sunlight utilization balance for cultivation and electrical energy generation as a function of the blind rotation threshold irradiance.

2. Model greenhouse

A model glass greenhouse was designed based on the structure and dimensions of an actual experimental greenhouse with floor area of 24 m^2 (5.65 m × 4.25 m) (Fig. 1). The model greenhouse is covered with 85% transmittance glass. The roof slope is 26.5°. The PV blinds [32] are assumed to be installed under the entire roof. To cover the entire roof area, 198 PV modules of 0.1 m^2 area each are used. Nevertheless, complete roof coverage with the actual PV blinds is difficult because of the high manufacturing cost of the custom-made semi-transparent PV modules. For this reason, in this study, only three PV modules were installed to the roof for the performance test. Complete performance with the full PV roof coverage was estimated by calculation based on data obtained from the triple PV module blind experiments.

A block diagram of the PV blind system for calculation is presented in Fig. 2. The three PV modules can be rotated using a single DC motor (SS23F-LH-860-DC12V; Sawamura Denki Ind. Co., Ltd., Kanagawa, Japan), which is used for the system validation experiments presented in Section 4. Accordingly, 66 DC motors were assumed to be necessary to rotate the 198 PV modules. The single DC motor rated current is 0.3 A. To rotate the three PV modules, 1 A of instantaneous maximum current is required. A DC motor full bridge driver (TB6643KQ; Toshiba Corp., Tokyo, Japan) is used to control the motor rotation direction. The maximum output current of the DC motor driver is 4.5 A. Therefore, one DC motor driver can control up to four DC motors. The motor control circuit is connected to a charge–discharge controller (SA-MN05-8; Denryo Co. Ltd., Tokyo, Japan) with 8.5 A of rated load current. The single charge–discharge controller can provide load current up to two DC motor drivers. To extend the PV-blind system to the whole greenhouse roof, 9 charge–discharge controllers and 18 DC motor drivers are assumed to be necessary. In principle, iterative deployment of the PV blind system portrayed in Fig. 2 enables application to larger-scale greenhouses. However, capacity optimization of the respective electrical and mechanical parts is necessary prior to large-scale application because the prototype system consists of over-functionalized components. For that reason, it is less cost efficient.

The size of each semi-transparent PV module used as the blind blade is 500 mm × 200 mm × 11 mm (Fig. 3a) with a three-layer structure

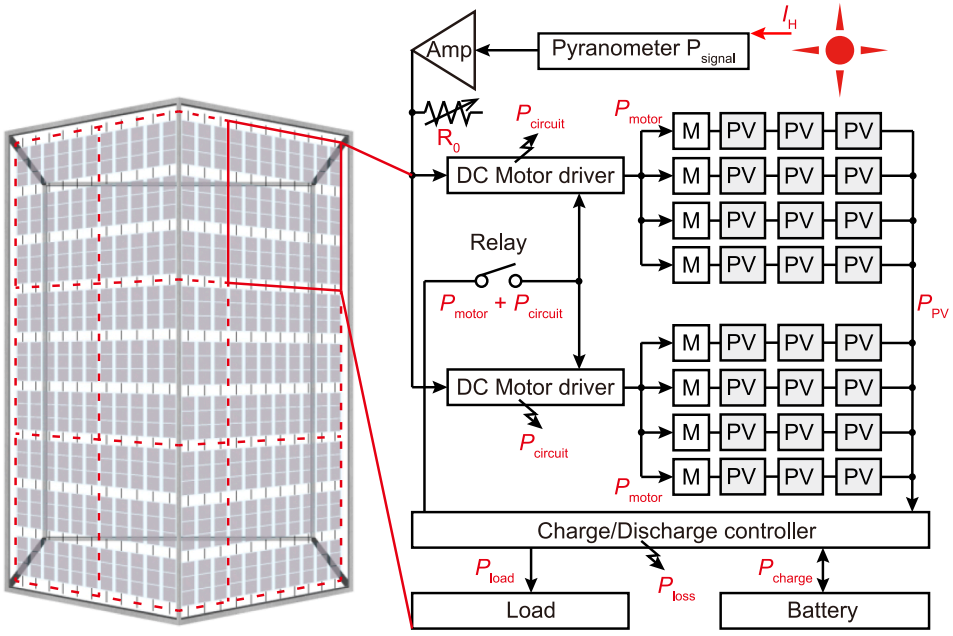

Fig. 2. Block diagram of the whole-roof PV-blind greenhouse, necessitating 9 charge–discharge controllers, 18 DC motor drivers, and 66 DC motors. M: DC motor.

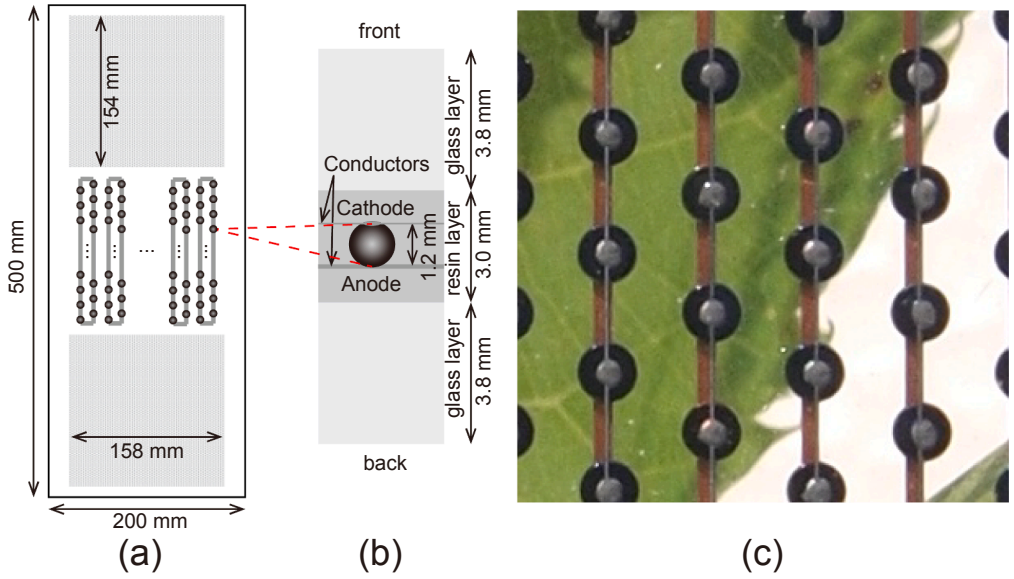

Fig. 3. Overview of the semi-transparent PV module (a) and its cross-sectional structure (b). Black dots represent micro-spherical solar cells. Sunlight passes through the module via cell–electrode interstices (c).

comprising glass, resin, and glass layers. In all, 13,764 spherical micro-PV cells (Sphelar®; Sphelar Power Corp., Kyoto, Japan) were embedded in the resin layer of the single PV module. The cathode of each PV cell was connected to a 0.1 mm-wide diameter conductor. The anode was connected to a 0.38 mm–wide wire (Fig. 3b). The 0.1 mm diameter conductor side was defined as the front surface of the semi-transparent PV module.

The motor drive circuit turns the PV blind in response to irradiance variation [32]. A pyranometer P_{signal} (ML-01; Eko Instruments Co. Ltd., Tokyo, Japan) transforms global horizontal irradiance I_H into the input signal voltage to the control circuit. An operational amplifier (LM358; Texas Instruments Inc., Texas, USA) linearly amplifies the P_{signal} output voltage. The amplification factor is regulated by the value of a variable resistor R_0 that is connected to the operational amplifier. The output voltage of the operational amplifier drives the DC motor full bridge driver to control the motor rotation direction. A threshold I_H value $I_{threshold}$ for triggering the blind rotation can be set by adjusting the R_0 value. The PV blind rotation stops at a position parallel ($\theta = 0°$) or perpendicular ($\theta = 90°$) to the roof when the PV blind touches a mechanical switch. When I_H exceeds a predetermined $I_{threshold}$, the PV blinds become oriented parallel to the roof to produce a greater amount of electricity with moderate sunlight shading by virtue of the PV module's semi-transparency. The PV blinds become oriented perpendicular to the roof when the irradiance level is lower than the $I_{threshold}$, prioritizing the sunlight intake into the greenhouse for crop cultivation (Fig. 4).

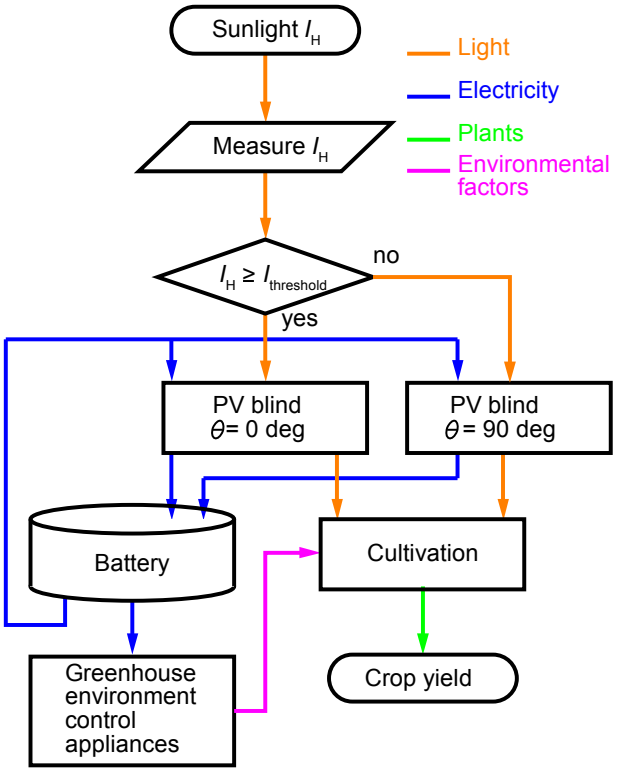

Fig. 4. Concept of the semi-transparent PV greenhouse shading control depicted as a flowchart.

3. Electrical energy generated by the PV blind under various sunlight conditions

3.1. Calculation of solar irradiance impinging on the PV blind and theoretically producible electric power

The theoretical annual solar irradiance as a continuous function of the time t (s) is calculated assuming a cloudless sky from 00:00:00 of January 1. The angle of the sun observed from the PV blind in the process of the earth's motion relative to the sun is presented in Fig. 5 in a polar coordinate system. The true solar time *TST* (hour) [45,46] is given as

$$TST = \frac{t}{3600} - 24\cdot(T-1) + \frac{\psi - 135.0}{15} + \frac{e}{60}, \tag{1}$$

where T (day) represents the number of days elapsed from 1 January ($T = 1$), ψ denotes the longitude of the university campus (133.1°), 135.0° stands for the longitude of Japan standard time, and e (min) is the equation of time given as [45,46]

$$e = 2.292\cdot\left[\begin{array}{c} 0.0075 + 0.1868\cdot\cos\left(\frac{2\pi(T-1)}{365}\right) - 3.2077\cdot\sin\left(\frac{2\pi(T-1)}{365}\right) \\ -1.4615\cdot\cos\left(\frac{4\pi(T-1)}{365}\right) - 4.089\cdot\sin\left(\frac{4\pi(T-1)}{365}\right) \end{array}\right] \tag{2}$$

The solar declination [45,47] δ (rad) and the hour angle [46,47] ω (rad) are given respectively as

$$\delta_t = \frac{23.45}{180}\cdot\pi\cdot\sin\left(2\pi\cdot\frac{284+T}{365}\right) \tag{3}$$

and

$$\omega_t = 15\cdot\frac{\pi}{180}\cdot(TST - 12). \tag{4}$$

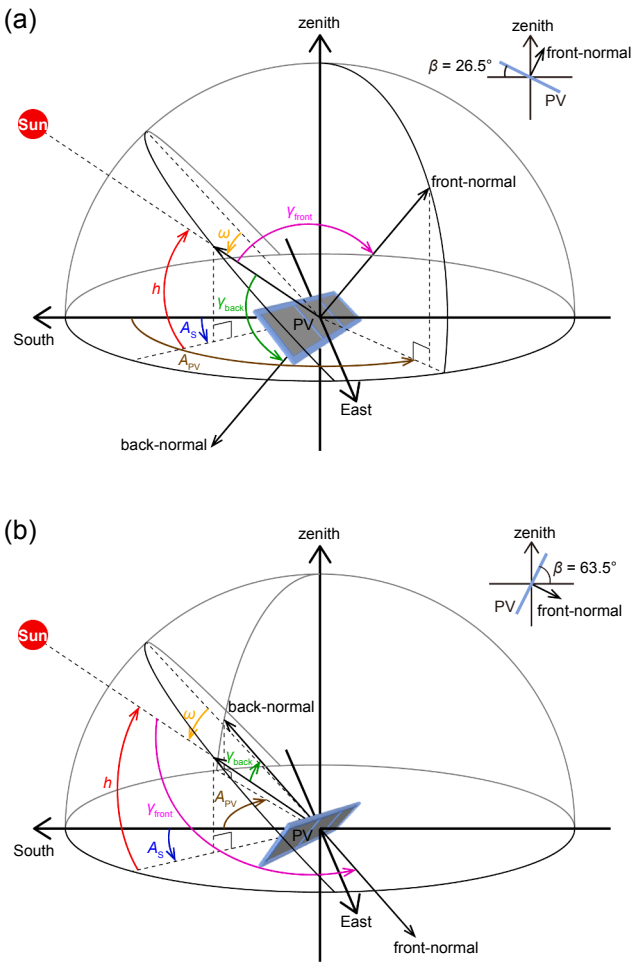

Fig. 5. Astronomical time-dependent parameters for calculating solar irradiances: $\theta = 0°$ (a) and $\theta = 90°$ (b), where θ stands for the angle between the PV blind surface and the greenhouse roof surface.

The solar altitude h (rad) is then calculated as [45,46,47]

$$h_t = arcsin(sin(\varphi)sin(\delta_t) + cos(\varphi)cos(\delta_t)cos(\omega_t)), \tag{5}$$

where $\varphi = 0.62$ rad $= 35.5°$ represents the latitude of the university campus. The solar azimuth A_S (rad) is then given as [45,46,47]

$$A_{S,t} = \begin{cases} -\arccos\left(\frac{\sin(h_t)\cdot\sin(\varphi) - \sin(\delta_t)}{\cos(h_t)\cdot\cos(\varphi)}\right) & (\omega_t < 0) \\ 0 & (\omega_t = 0) \\ \arccos\left(\frac{\sin(h_t)\cdot\sin(\varphi) - \sin(\delta_t)}{\cos(h_t)\cdot\cos(\varphi)}\right) & (\omega_t > 0) \end{cases} \tag{6}$$

The PV module inclination β (deg) is

$$\beta_t = \begin{cases} 26.5° & (\theta_t = 0°) \\ 63.5° & (\theta_t = 90°) \end{cases}. \tag{7}$$

Only these two β values are considered for this study. The angle γ_{front} (rad) between the direct beam sunlight on the PV blind and the PV blind front-normal is [46,47]

$$\gamma_{front,t} = \begin{cases} arccos\left(\begin{array}{c} sin(h_t)\cdot cos(\beta_t) \\ +cos(h_t)\cdot sin(\beta_t)\cdot cos(A_{S,t} - A_{PV,t}) \end{array}\right) & (\theta_t = 0°) \\ \pi - \arccos\left(\begin{array}{c} \sin(h_t)\cdot\cos(\beta_t) \\ +\cos(h_t)\cdot\sin(\beta_t)\cdot\cos(A_{S,t} - A_{PV,t}) \end{array}\right) & (\theta_t = 90°) \end{cases}, \tag{8}$$

where A_{PV} stands for the azimuth of the PV blind's sky facing surface.

Table 1
Atmospheric transmittance monthly average values during 1971–2000 in Yonago.*

January	February	March	April	May	June	July	August	September	October	November	December
0.73	0.69	0.64	0.62	0.61	0.62	0.61	0.62	0.66	0.69	0.72	0.74

*Yonago is the closest reference city to Matsue for statistical data of atmospheric transmittance [50].

When the PV blind oriented itself from $\theta = 0^\circ$ to $\theta = 90^\circ$, A_{PV} increased to $A_{PV} + \pi$. The range of azimuth angles A_S and A_{PV} is $[-\pi, \pi)$. True south is defined as 0 rad of the azimuth angle, which has positive values to the west.

The angle γ_{back} (rad) between the direct beam sunlight irradiating on the PV blind and the PV blind back-normal is calculated as

$$\gamma_{back,t} = \pi - \gamma_{front,t}. \tag{9}$$

The direct irradiance on a horizontal surface I_{direct} (W m^{-2}) is

$$I_{direct,t} = \begin{cases} 0 & (h_t \leqslant 0) \\ I_0 p^{\frac{1}{\sin(h_t)}} \sin(h_t) & (h_t > 0) \end{cases} \tag{10}$$

Here, $I_0 = 1.37 \times 10^3$ W m^{-2} is the solar constant; p is the atmospheric transmissivity. The diffuse irradiance on a horizontal surface $I_{diffuse}$ (W m^{-2}) is given as [47,48,49]

$$I_{diffuse,t} = \begin{cases} 0 & (h_t \leqslant 0) \\ \dfrac{I_0 \sin(h_t)\left(1 - p^{\frac{1}{\sin(h_t)}}\right)}{2(1 - 1.4 \ln p)} & (h_t > 0) \end{cases} \tag{11}$$

Monthly average p values of the nearest observation site from the experimental greenhouse are presented in Table 1. The global irradiance on the horizontal surface I_H (W m^{-2}) is calculated as

$$I_{H,t} = I_{direct,t} + I_{diffuse,t}. \tag{12}$$

The direct irradiance on the PV blind front-surface $I_{front\ direct}$ (W m^{-2}) and back-surface $I_{back\ direct}$ (W m^{-2}) are given as

$$I_{a\ direct,t} = \begin{cases} I_0 p^{\frac{1}{\sin(h_t)}} \cos(\gamma_{a,t}) & (h_t > 0,\ \gamma_{a,t} < \dfrac{\pi}{2}) \\ 0 & (h_t \leq 0 \text{ or } h_t > 0,\ \gamma_{a,t} \geq \dfrac{\pi}{2}) \end{cases} \tag{13}$$

Here, subscript "a" represents "front" or "back". Assuming that the diffuse irradiance is distributed isotropically over the sky dome, the diffuse irradiances on the PV blind front-surface $I_{front\ diffuse}$ (W m^{-2}) and on the PV blind back-surface $I_{back\ diffuse}$ (W m^{-2}) are given as the following [45]:

$$I_{b\ diffuse,t} = \begin{cases} 0 & (h_t \leqslant 0) \\ \dfrac{I_{diffuse,t}(1 \pm cos(\beta_t))}{2} & (h_t > 0, \theta_t = 0^\circ) \\ \dfrac{I_{diffuse,t}(1 \mp cos(\beta_t))}{2} & (h_t > 0, \theta_t = 90^\circ) \end{cases}, \tag{14}$$

where subscript "b" represents "front" ("+" is chosen in the second line and "−" in the third line) or "back" ("−" is chosen in the second line and "+" in the third line). The ground-reflected irradiances on the PV blind front-surface $I_{front\ reflect}$ (W m^{-2}) and back-surface $I_{back\ reflect}$ (W m^{-2}) are given as

$$I_{c\ reflect,t} = \begin{cases} 0 & (h_t \leqslant 0) \\ \dfrac{\rho \cdot I_{H,t}(1 \mp cos\beta_t)}{2} & (h_t > 0, \theta_t = 0^\circ) \\ \dfrac{\rho \cdot I_{H,t}(1 \pm cos\beta_t)}{2} & (h_t > 0, \theta_t = 90^\circ) \end{cases} \tag{15}$$

Here, subscript "c" represents "front" ("−" is chosen in the second line and "+" in the third line) or "back" ("+" is chosen in the second line and "−" in the third line); ρ is the ground albedo, which is assumed to be a constant value of 0.10. Based on the calculation of these solar irradiances, the global irradiances on the PV front surface I_{front} (W m^{-2}) and on the back surface I_{back} (W m^{-2}) can be calculate as

$$I_{d,t} = \varepsilon\left(I_{d\ direct,t} + I_{d\ diffuse,t} + I_{d\ reflect,t}\right) \tag{16}$$

Here, subscript "d" represents "front" or "back"; $\varepsilon = 0.85$ is the transmittance coefficient of the greenhouse glass.

The producible maximum electric power of the single PV module P_{max} (W) based on its single-side area S_{PV} (m^2) is calculated as [51]

$$P_{max,t} = \frac{\eta_{M,t} \cdot S_{PV}(I_{front,t} + I_{back,t})}{100}, \tag{17}$$

where η_M (%) represents the PV module efficiency.

3.2. Validating electrical characteristics of the PV-blind with respect to the impinging sunlight angle

The electrical characteristics of the PV module (Appendix A) with various PV orientations and inclination angles were measured at a field plot on the Shimane University campus on 27 and 31 July, 2–4 August, 8, 13, and 14 September 2017 (Table A1).

The PV module was supported 2 m above the ground by a cubical framework. The PV module was fixed to a rotatable metal shaft. Therefore, it can be adjusted to different inclination angles. Two pyranometers P_{front} and P_{back} (ML-01) were mounted on the shaft so that the P_{front} normal coincided with the PV module front normal, and the P_{back} faced 180° opposite. The global irradiances on the top PV surface I'_{front} and the bottom surface I'_{back} were measured respectively using P_{front} and P_{back}. Pyranometer P_H (ML-01) was mounted on the top of the cubical framework to measure I'_H.

Using a data acquisition unit (34970A; Agilent Technologies Inc., California, USA), I'_H, I'_{front}, and I'_{back} were recorded at 1 min intervals. The current (i'_{PV})–voltage (V'_{PV}) characteristics of the PV module were measured at 1 min intervals using a voltage and current source/meter (6241A; ADC Corp., Tokyo, Japan). Data were transmitted through the GPIB interface and were stored in a computer.

The weather was fine on 27 and 31 July, 3 August, and 13 September. It was partially cloudy on other days. The PV inclination angle β was 26.5° on prior four days during which the PV module front normal faced to the sky, whereas the front normal faced the ground on the latter four days: $\beta = 63.5^\circ$. For that reason, I'_{front} was greater than I'_{back} on the prior four days (Fig. A1a–d), whereas I'_{back} was greater than I'_{front} on the latter four days (Fig. A1e–h). Because of the bifacial structure, not only did irradiance impinge on the upper side of the PV module, but the impingement on the bottom side was effective for electricity production. For instance, on 27 July (Fig. A1a), the backside also contributes to harvesting of sunlight, resulting in greater sunlight accumulation by the PV module. The merit of the PV bifaciality is emphasized for greenhouse applications because all roofs and walls are transparent. The percentage of contribution of the bottom side varies with the PV module bearing. For instance, the bottom side irradiation reached 17–28% of the top side irradiation when the PV module front side faced the southern sky (Fig. A1a). The percentage became 100% at the intersections of I'_{front} and I'_{back} curves as recorded on 4 August (Fig. A1e) and on 13 September (Fig. A1g) when $\gamma_{front} = \gamma_{back} = 90^\circ$. Merits of the bifacial PV structure are apparent at such times.

The current–voltage and power–voltage characteristics of the single

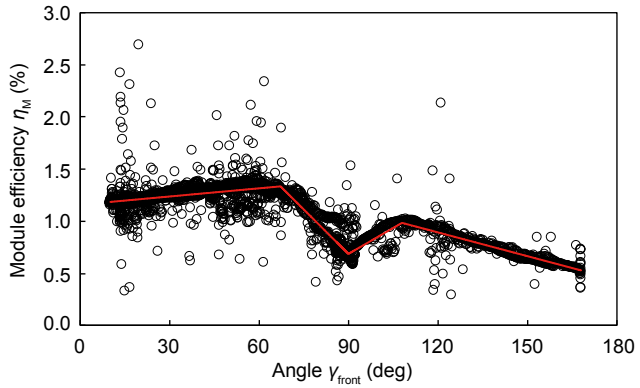

Fig. 6. Relation between γ_{front} and experimentally obtained η_M. Regression lines are depicted as red solid lines. (For interpretation of the references to colour in this figure legend, the reader is referred to the web version of this article.)

PV module measured on 3 August 2017 are presented in Fig. A2. The maximum value of each power output P'_{PV} curve (Fig. A2b) is defined as P'_{max}. Relations between P'_{max} and $I'_{front} + I'_{back}$ on each day are presented in Fig. A3. The values of P'_{max} increased with $I'_{front} + I'_{back}$. However, the relation between P'_{max} and $I'_{front} + I'_{back}$ was not simply linear. For $\beta = 26.5°$ (Fig. A3a–d), P'_{max} increased with $I'_{front} + I'_{back}$. However, the slope of P'_{max} was suppressed when $\beta = 63.5°$ (Fig. A3e–h). This inconsistent behavior of P'_{max} against the input irradiance is explainable by the asymmetric width of the PV module wires. As depicted in Fig. 3, the anode-side wire was wider than the cathode wire. Accordingly, P'_{max} was suppressed by the anode-wire partial shadow on each solar cell when the anode-side faced to the sky (Fig. A3e–h). The maximum P'_{max} value was 1.88 W ($V_{PV} = 15.6$ V, $i_{PV} = 120.8$ mA) at 11:31 on 2 August (Fig. A3c).

The PV module efficiency η_M (%) can be determined as

$$\eta_M = \frac{P'_{max}}{S_{PV}(I'_{front} + I'_{back})} \times 100. \quad (18)$$

Nevertheless, the determination of η_M by calculation was not easy because P'_{max} was affected by the module structure, including sunlight reflection on the module cover glass and the asymmetric partial shading by the wires. Direct sunlight impinges the PV-module front surface when $0 \le \gamma_{front} < 90°$, whereas it impinges the back surface when $90° < \gamma_{front} \le 180°$. Because the conductor width on the PV module back side was wider than that on the front side, η_M values of $90° < \gamma_{front} \le 180°$ were less than those of $0 \le \gamma_{front} < 90°$ (Fig. 6). The conductors partially shaded the PV cells from direct sunlight irradiating from the module normal directions. For this reason, η_M decreased when γ_{front} approached to 0° or 180°. The critical angles of light impinging from air to the PV-module cover glass are determined to be $\gamma_{front} = 67°$ and 108°. The total internal reflections occurred at the medium boundaries when $67° < \gamma_{front} \le 108°$. When $\gamma_{front} = 67°$, η_M reached the maximum value of 1.4%. The PV module generated electricity using diffused and reflected irradiance with low module efficiency ($\eta_M = 0.69\%$) when $\gamma_{front} = 90°$.

Instead of formula 18, η_M had a correlation with γ_{front} as determined using data obtained through the experiments (Fig. 6). The values of η_M increased gradually with γ_{front} from 0° to 67°, and then decreased steeply until $\gamma_{front} = 90°$. It rebounded at $\gamma_{front} = 90°$ and decreased again with γ_{front} from 108° to 180°. These optical conditions suggest the piece-wise linear changes of η_M. Therefore, η_M was identified as the piece-wise linear function using least squares approximation as shown below:

$$\eta_{M,t} = \begin{cases} 2.6 \times 10^{-3}\gamma_{front,t} + 1.2 & (0 \leqslant \gamma_{front,t} \leqslant 67°) \\ -2.9 \times 10^{-2}\gamma_{front,t} + 3.3 & (67° < \gamma_{front,t} \leqslant 90°) \\ 1.7 \times 10^{-2}\gamma_{front,t} - 0.81 & (90° < \gamma_{front,t} \leqslant 108°) \\ -7.6 \times 10^{-3}\gamma_{front,t} + 1.8 & (108° < \gamma_{front,t} \leqslant 180°) \end{cases} \quad (19)$$

The coefficient of determination between the calculated η_M using the linear equation and the experimental data is $R^2 = 0.81$. Although no experimental data were obtained, η_M around $\gamma_{front} = 0°$ and 180° can be regarded conservatively as applicable to the formulated equation (19). The P_{max} value can be estimated from γ_{front} and $I_{front} + I_{back}$ using Eqs. (17) and (19).

4. Electrical energy balance of the PV-blind roof system

4.1. Electrical energy balance equation

The energy balance of the PV blind system was calculated through development of an ordinary differential equation model. Based on energy-budget considerations, the equation is set as

$$P_{charge,t} = \frac{de_{charge}}{dt} = n \cdot P_{PV,t} - m \cdot P_{motor,t} - l \cdot P_{circuit,t} - P_{load,t} - k \cdot P_{loss,t}, \quad (20)$$

where de_{charge} represents the energy charged into the battery during infinitesimal time interval dt. Other variables P_{charge}, P_{PV}, P_{motor}, $P_{circuit}$, P_{load}, and P_{loss} respectively denote the power charged into the battery, the single PV generated power, single DC motor control power, single motor-control-circuit power, load power consumption, and system power loss. Here, P_{loss} is attributed mainly to power consumption by the charge–discharge controller. Coefficients n, m, l, and k respectively represent the numbers of PV modules, DC motors, motor control circuits, and charge–discharge controllers. The values of P_{PV}, P_{motor}, $P_{circuit}$, P_{load}, and P_{loss} are greater than or equal to 0. Negative P_{charge} means that the

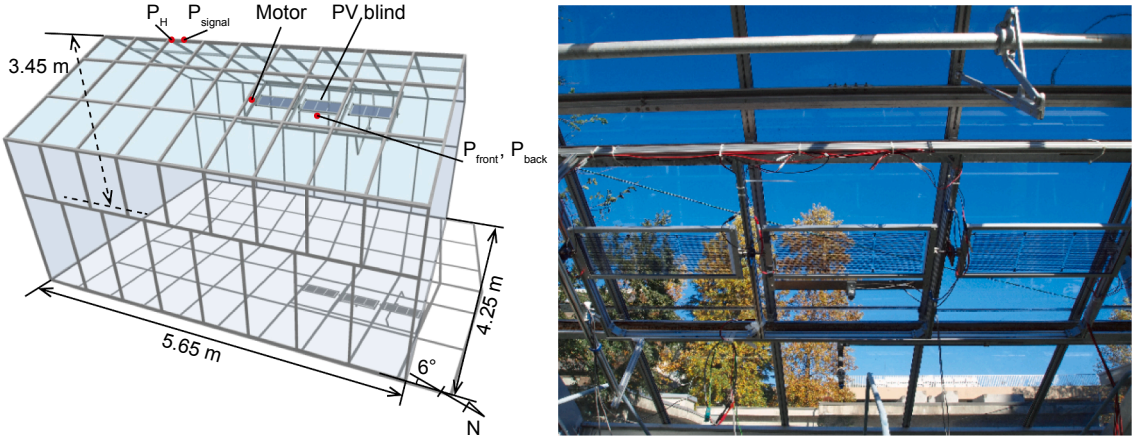

Fig. 7. Prototype PV blind system installed underneath the experimental greenhouse glass roof facing the eastern sky.

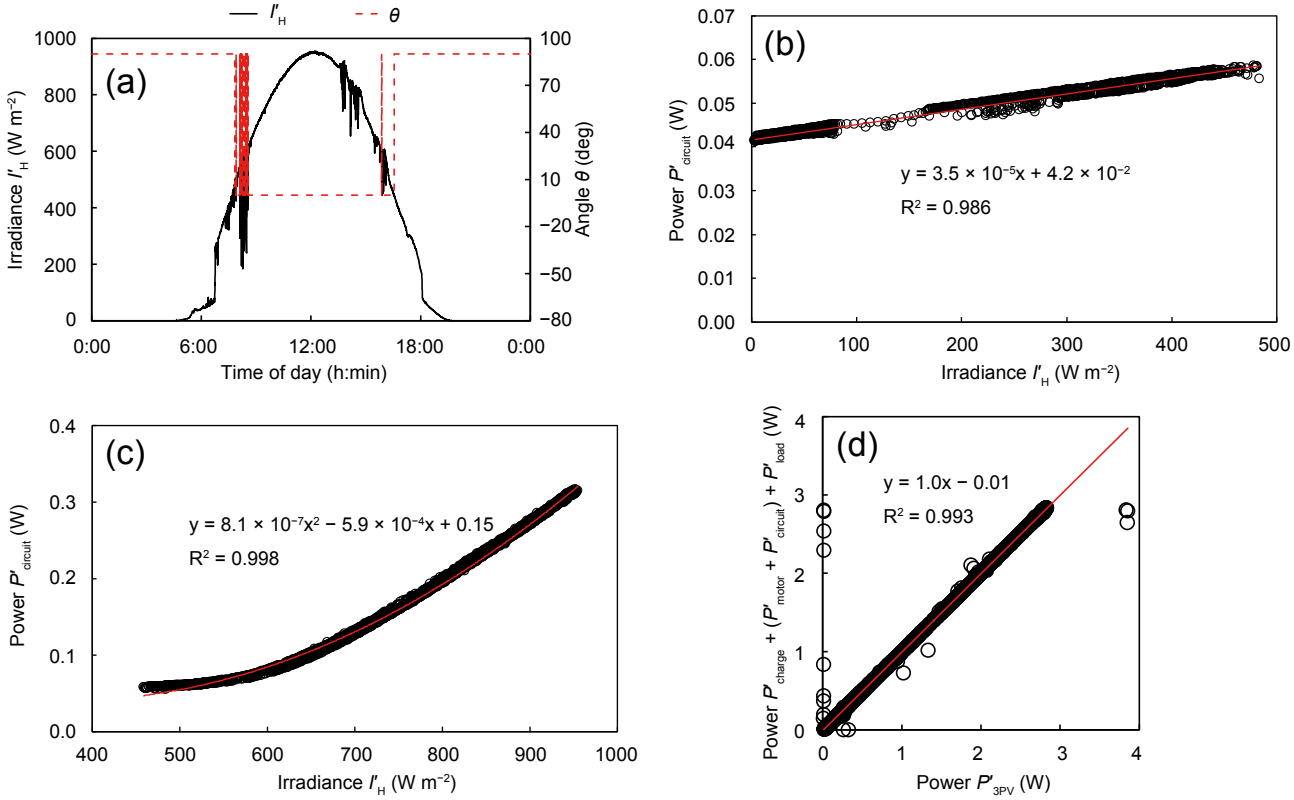

Fig. 8. Data obtained on 24 June 2018 used to determine power parameters related to the system operation: measured irradiance I'_H and angle θ (a); fitting lines (red solid lines) for the relation of measured power $P'_{circuit}$ and I'_H when θ was 90° (b) and 0° (c); relation between P'_{charge} + (P'_{motor} + $P'_{circuit}$) + P'_{load} and P'_{3PV} (d).

battery is in a discharge state (Fig. 2). We can calculate the energy balance in the present PV system by integrating equation (20) with respect to the time subjected to an initial condition. This procedure requires specification of each term of the equation based on observable variables, which have been identified using experimentally obtained data and theoretical considerations.

4.2. Tests of the prototype greenhouse PV-blind system performance to obtain necessary parameters to solve the energy balance equation

To obtain necessary parameters to estimate the energy balance of whole-greenhouse PV-blind operations, a prototype PV-blind system with triple PV-modules was installed to the experimental greenhouse on the Shimane University Matsue campus (35°29′ N, 133°04′ E) (Fig. 7). The 198-PV-module blind system performance (Fig. 2) was estimated multiplicatively based on parameters obtained from experimental data.

Pyranometers P_H and P_{signal} (ML-01) were positioned on the greenhouse apex to measure I'_H. The P_{signal} output cables were connected to the DC-motor (SS23F-LH-860-DC12V) control circuit (Fig. 2). Its output voltage was used as the signal to determine the PV-blind rotation direction in response to I'_H. Pyranometers P_{front} and P_{back} (ML-01) were installed proximally at the bottom long side of the middle PV module. The P_{front} and P_{back} normals were set respectively to coincide with the PV module front and back normals. The global irradiances on the PV-blind front surface I'_{front} and on the back surface I'_{back} were measured respectively using P_{front} and P_{back}.

The triple PV modules, the control circuit, a battery with 50 Ah rated capacity (JC50-12; Denryo Co. Ltd., Tokyo, Japan), and a load consisted of light-emitting diodes (LEDs, HLMP-1540; Broadcom Inc., San Jose, CA, USA) were connected to the charge–discharge controller (SA-MN05-8) (Fig. 2). The PV blind system was operated during a year from 8 December 2017 through 7 December 2018, excepting some maintenance days on 10–13 July, 17 September, 25 October, and 19 November. The LED-load had been connected 24 h per day from 14 February through 19 November in 2018 to avoid saturation of the battery charging capacity by PV generated electricity during summer. The three PV modules were connected electrically in parallel to the charge–discharge controller. The currents generated by the three PV modules (i'_{3PV}), charged the battery (i'_{charge}), supplied the motor control circuit with the DC motor (i'_{motor} + $i'_{circuit}$), and supplied the LED-load (i'_{load}), the voltages at the three PV modules (V'_{3PV}), the battery (V'_{charge}), and the charge–discharge controller load terminal ($V'_{discharge}$), and the solar irradiances I'_H, I'_{front}, and I'_{back} were measured at 10 s intervals using a data acquisition unit (34972A; Keysight Technologies Inc., Santa Rosa, CA, USA). The three PV modules were assumed to have the same operating current and voltage under the same conditions i_{3PV} = 3i_{PV} and V_{3PV} = V_{PV}, and P_{3PV} = 3P_{PV}. Eq. (20) in the prototype PV-blind system becomes

$$P_{charge,t} = \frac{de_{charge}}{dt} = P_{3PV,t} - \left(P_{motor,t} + P_{circuit,t}\right) - P_{load,t} - P_{loss,t}. \quad (21)$$

The PV blind was rotated between the parallel (θ = 0°) and perpendicular (θ = 90°) angles to the greenhouse roof. When the I'_H value was greater than or equal to $I_{threshold}$, the PV blind was oriented parallel to the greenhouse roof. The PV blind was oriented perpendicular to the roof when I'_H was less than $I_{threshold}$. Therefore,

$$\theta_t = \begin{cases} 0° & \left(I_{H,t} \geqslant I_{threshold}\right) \\ 90° & \left(I_{H,t} < I_{threshold}\right) \end{cases} \quad (22)$$

Throughout the experimental period, $I_{threshold}$ was set as 500 W m^{-2}.

4.3. Determination of electrical power in the energy balance equation

The sunny day nearest to the summer solstice was June 24, 2018. Therefore, data obtained on that day were used to determine the power parameters related to the motor control circuit. The electricity power

consumption of the motor control circuit $P'_{motor} + P'_{circuit}$ (W) can be decomposed into P_{motor} and $P_{circuit}$. Through analysis of experimentally obtained data, $P_{circuit}$ was formulated. The PV blind rotations and I'_H are presented in Fig. 8a. The PV blind was rotated 31 times during 7:49–8:33 and three times during 15:52–16:33. The $P'_{motor} + P'_{circuit}$ value was ascertained as the product of $V'_{discharge}$ and $i'_{motor} + i'_{circuit}$. During nighttime, the relay disconnected the motor control circuit. Thereby $P'_{motor} + P'_{circuit} = 0$. Because the output signal of the operational amplifier varies with I'_H (Fig. 2), $P'_{circuit}$ is related to I'_H. The relation between $P'_{circuit}$ and I'_H during the blind standby condition is depicted in Fig. 8b and c. One amplifier, two transistors, multiple resistors, and one motor driver exist in the single motor control circuit [32]. Electric current distribution in the control circuit changes according to θ. Consequently, $P'_{circuit}$ differed between $\theta = 0°$ and 90° conditions. When $\theta = 90°$, $P'_{circuit}$ was proportional to I'_H. In contrast, $P'_{circuit}$ was not proportional to I'_H when $\theta = 0°$. Based on experimentally obtained data, $P_{circuit}$ was expressed as a function of I_H:

$$P_{circuit,t} = \begin{cases} 0 & (I_{H,t} = 0) \\ 3.5 \times 10^{-5} I_{H,t} + 4.2 \times 10^{-2} & (I_{H,t} > 0,\ \theta_t = 90°) \\ 8.1 \times 10^{-7} I_{H,t}^2 - 5.9 \times 10^{-4} I_{H,t} + 0.15 & (I_{H,t} > 0,\ \theta_t = 0°) \end{cases} \quad (23)$$

Our earlier study [32] already determined P_{motor} (W) experimentally as

$$P_{motor} = \begin{cases} 3.1 & (\text{during a blind turn}) \\ 0 & (\text{standby}) \end{cases} \quad (24)$$

The LED-load had consumed constantly $P'_{load} = 0.37$ W. The P'_{3PV} value was calculated as the product of V'_{3PV} and i'_{3PV}. The sum of P'_{charge}, $P'_{motor} + P'_{circuit}$, and P'_{load} has positive correlation with P'_{3PV} (Fig. 8d). Their relation is expressed as

$$P'_{charge} + (P'_{motor} + P'_{circuit}) + P'_{load} = 1.0 \times P'_{3PV} - 0.01. \quad (25)$$

Comparison of Eq. (25) with Eq. (21) indicates P_{loss} as 0.01 W. P_{PV} (W) is estimated as

$$P_{PV,t} = \begin{cases} \kappa P_{max,t} & h_t > 0 \\ 0 & h_t \le 0 \end{cases} \quad (26)$$

Actually, P_{PV} represents the actual output of the single PV module when connected to the system. Conversion coefficient κ between P_{max} and P_{PV} was calculated using one-year experimental data as

$$\kappa = \frac{\int_M P'_{3PV} dt}{\int_M \frac{3 \cdot S_{PV} \cdot \eta_{M,t} \cdot (I'_{front} + I'_{back})}{100} dt} = 0.74. \quad (27)$$

Therein, M is the set of measurement times t when $h_t > 0$ with 10 s intervals from 8 December 2017 through 7 December 2018.

4.4. Electrical energy calculation of the triple PV-module blind installed in the experimental greenhouse

The prototype PV blind was rotated automatically 16,138 times during 358 days. The PV blind turned when I'_H (mean ± SD) was 508.47 ± 163.19 W m^{-2}. Using a forward-Euler [52] discretized counterpart of the established mathematical model, I_H, I_{front}, I_{back}, P_{PV}, $P_{circuit}$, and P_{motor} are calculatable at arbitrary times t during one year under a cloudless sky condition. Then, an artificial coefficient μ was introduced to compensate for the error between the calculated model and measured data that include the actual cloudy-sky condition. Coefficient μ is expressed by the following formula based on the measured I'_H and calculated I_H:

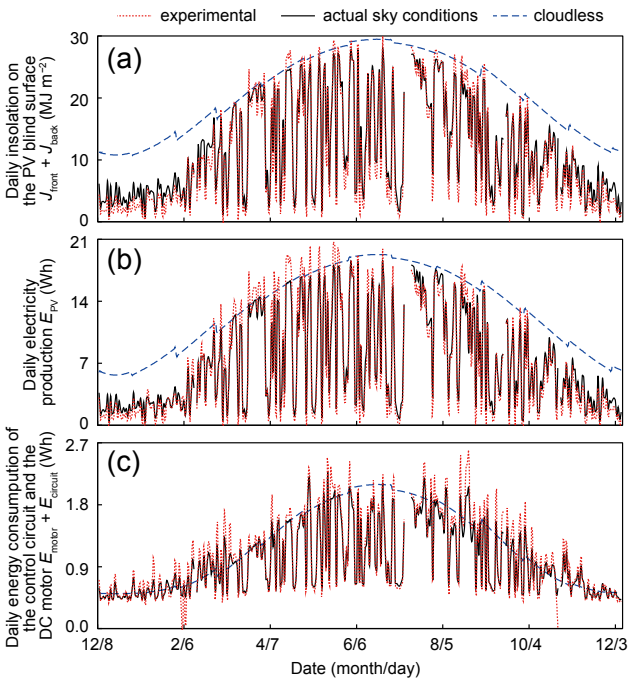

Fig. 9. Calculated and measured daily insolation and electrical energies when $I_{threshold} = 500$ W m^{-2} at the experimental greenhouse: insolation on the PV blind surface $J_{front} + J_{back}$ (MJ m^{-2}) (a); electricity production E_{PV} (Wh) (b); energy consumption of the control circuit and the DC motor $E_{motor} + E_{circuit}$ (Wh) (c).

$$\mu_t = \begin{cases} 0 & (I_{H,t} = 0) \\ min\left\{\frac{I'_H}{I_{H,t}}, 1.0\right\} & (I_{H,t} > 0) \end{cases} \quad (28)$$

The actual sky condition can be incorporated into the calculation using μ. Under a partial cloudy sky with visible sun, I'_H can exceed the theoretical cloudless sky I_H because refraction and reflection of direct sunlight on cloud edges irradiate the greenhouse in addition to the direct beam sunlight. In this case, μ can be effectively replaced by 1.0. Irradiance I_H is compared with $I_{threshold} = 500$ W m^{-2} to ascertain the time of each PV blind turn.

The P_{max} value was calculated using Eqs. (17) and (19). Insolation values originating from I_H and $I_{front} + I_{back}$ are denoted respectively as J_H and $J_{front} + J_{back}$ (MJ m^{-2}). Surplus energy, battery charged energy, energy generated by the triple PV-module blind, energy consumed by the motor control circuit with the DC motor, and the system energy loss are denoted respectively as $E_{surplus}$, E_{charge}, E_{PV}, $E_{motor} + E_{circuit}$, and E_{loss}. When no load is connected to the system, $E_{surplus} = E_{charge}$.

Measured and calculated daily insolation and electrical energies when $I_{threshold} = 500$ W m^{-2} are presented in Fig. 9. Frequent partial cloud cover is common in the region of the study site. Therefore, daily $J'_{front} + J'_{back}$ and E'_{PV} varied frequently. The calculation based on the actual sky condition approximately reproduced the progress of experimentally obtained insolation and electrical energy. Calculated daily $J_{front} + J_{back}$ under the actual sky condition was slightly higher than the experimental data in winter (Fig. 9a). The solar altitude was low in winter. Consequently, the greenhouse was in building shadows in the early morning and late afternoon. The building shading was not considered in calculations. Therefore, the calculated $J_{front} + J_{back}$ values under the actual sky condition were greater than the measured values. Some sharp shifts appearing in the cloudless-sky calculation curves (blue dashed lines in Fig. 9) were caused by discontinuities of the monthly average atmospheric transmittance (Table 1). Daily $E'_{motor} + E'_{circuit}$ varied as affected by irradiance, but biased 0.5 Wh by which control

Table 2
Annual insolation and electrical energies when the blind rotation threshold irradiance was set at 500 W m^{-2} in the experimental greenhouse.

	Calculated under cloudless conditions (365 days)	Calculated under actual sky conditions (358 days)	Measured (358 days)
Annual global insolation J_H (MJ m^{-2})	7,098	4,146	4,321
Annual insolation on both surfaces of the PV module $J_{front} + J_{back}$ (MJ m^{-2})	6,769	3,751	3,437
Annual electricity production E_{PV} (kWh)	4.8	2.5	2.5
Annual energy consumption of the control circuit with the DC motor $E_{motor} + E_{circuit}$ (kWh)	0.44	0.35	0.37
Annual system energy loss E_{loss} (kWh)	0.09	0.09	0.09
Annual surplus electrical energy $E_{surplus}$ (kWh)	4.2	2.1	2.0
Number of blind rotations	730	16,114	16,138

circuit operations were maintained during day time. The control circuit disconnection from the blind system on 5 and 7 February and 24 October caused $E'_{motor} + E'_{circuit} = 0$.

Calculated and experimentally obtained annual energy of the prototype system when $I_{threshold} = 500$ W m^{-2} are presented in Table 2. The annual E_{PV} of the triple PV-module blind was estimated as 4.8 kWh under cloudless sky condition, in which the PV blind rotates only twice a day to keep them parallel to the roof surface when $I_H \geq 500$ W m^{-2}. In this ideal condition, the annual system energy consumption ($E_{motor} + E_{circuit} + E_{loss}$) was estimated as 0.5 kWh, which corresponds to 10% annual electricity production. By contrast, the calculated annual E_{PV} became 2.5 kWh under the actual sky condition. The annual $E_{motor} + E_{circuit}$ under the actual sky condition was 5% less than $E'_{motor} + E'_{circuit}$. The annual $E'_{motor} + E'_{circuit}$ value accounted for 15% of E'_{PV}. The system energy consumption was 0.4 kWh. Consequently, the estimated $E_{surplus}$ under the actual sky condition became half of that under the cloudless condition.

The annual system energy loss E_{loss} was estimated using the constant value of $P_{loss} = 0.01$ W (Eq. (25)). The value of E'_{loss} was 4% of E'_{PV} (Table 2). Calculated and measured annual cumulative surplus energy values are presented in Fig. 10. The annual $E'_{surplus}$ was 2.0 kWh. The annual $E_{surplus}$ under the actual sky condition was 2.1 kWh. The LED load consumed 2.7 kWh during 14 February through 19 November.

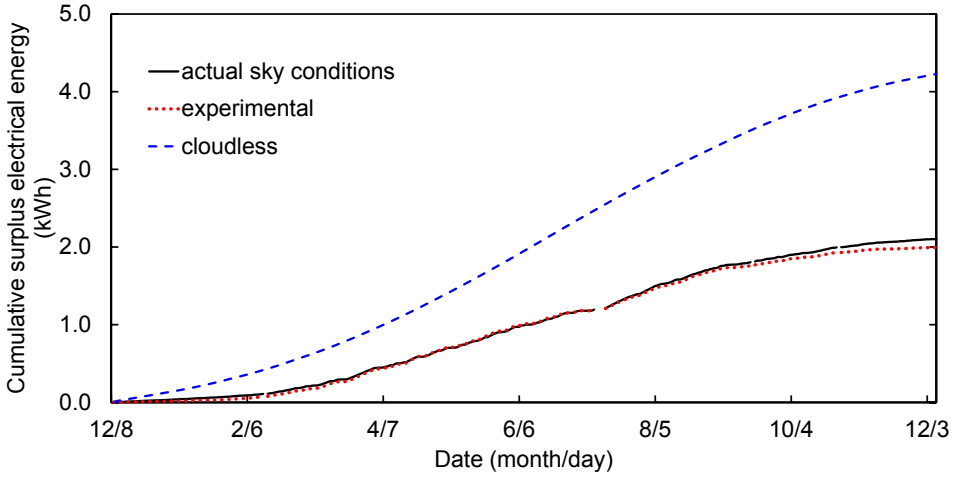

Fig. 10. Calculated and measured annual cumulative energy at the rotation threshold irradiance of 500 W m^{-2} at the experimental greenhouse.

Table 3
Estimation of annual electrical energy generation and surplus energy of the greenhouse whole-roof PV-blind system with different rotation threshold irradiances and greenhouse orientations under cloudless and actual sky conditions.

$I_{threshold}$ (W m^{-2})	Number of blind turns		E_{PV} per unit greenhouse area (kWh m^{-2})				$E_{surplus}$ per unit greenhouse area (kWh m^{-2})			
			Greenhouse orientation							
			N–S		E–W		N–S		E–W	
	a	b	a	b	a	b	a	b	a	b
0	0	0	13.42	7.83	13.25	7.76	13.01	7.45	12.84	7.39
100	730	4,656	13.43	7.81	13.27	7.72	13.06	7.50	12.90	7.41
200	730	8,578	13.53	7.68	13.26	7.54	13.17	7.35	12.90	7.21
300	730	13,552	13.67	7.48	13.16	7.25	13.31	7.10	12.80	6.87
400	730	16,984	13.72	7.29	12.96	6.95	13.35	6.87	12.60	6.53
500	730	16,114	13.35	7.04	12.62	6.64	12.98	6.64	12.25	6.24
600	546	13,262	12.57	6.69	12.02	6.28	12.21	6.32	11.66	5.91
700	454	10,248	11.68	6.22	11.19	5.83	11.33	5.88	10.84	5.48
800	364	7,458	10.59	5.66	10.13	5.27	10.27	5.36	9.80	4.97
900	236	3,356	9.26	5.01	8.81	4.61	8.99	4.76	8.53	4.37
1000	0	0	8.31	4.74	7.83	4.33	8.09	4.54	7.61	4.13

a, under cloudless sky conditions; b, under actual sky conditions.

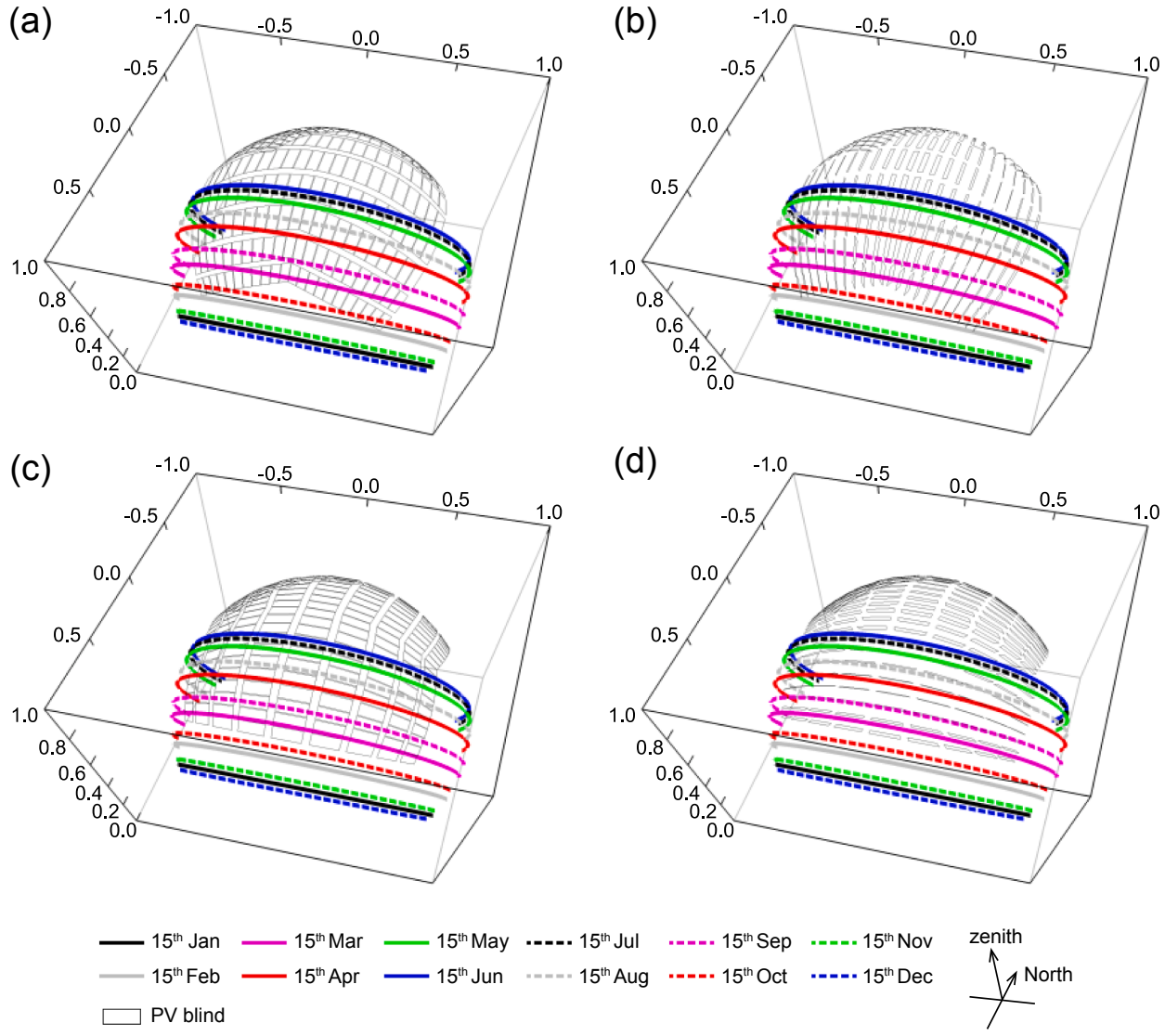

Fig. 11. The PV blind and sun path projections on the imaginary hemispherical surface for $\theta = 0^\circ$ (a, c) and 90° (b, d) in the north–south (a, b) and east–west (c, d) oriented PV-blind greenhouse, respectively. Direct sunlight paths of the 15th day of every month are presented.

4.5. Estimation of insolation allocation to PV electricity generation and crop production in the whole-roof PV-blind greenhouse

The annual electrical energies of the whole-roof PV-blind system of the model greenhouse (Fig. 2) were calculated under cloudless and actual sky conditions (Table 3). The geographic location was set at the experimental greenhouse. The model greenhouse ridge was assumed to be along true north–south (N–S) or east–west (E–W). The parameter $I_{threshold}$ was changed 0–1,000 W m^{-2} with 100 W m^{-2} intervals.

The PV blinds rotate twice a day when I_H exceeds the $I_{threshold}$ in the morning and declines in the afternoon under the cloudless sky condition. The PV blinds do not rotate throughout the year when $I_{threshold}$ is set at 0 W m^{-2} (always $\theta = 0^\circ$) or 1,000 W m^{-2} (always $\theta = 90^\circ$). The number of blind turns becomes 730 when $I_{threshold}$ is set below 500 W m^{-2}. The number decreases gradually when it is set higher than 500 W m^{-2}. The proportion of E_{motor} to E_{PV} does not exceed 0.6‰. When $I_{threshold} = 400$ W m^{-2}, E_{PV} reaches the maximum value of 13.7 kWh m^{-2} in the N–S oriented greenhouse. By contrast, E_{PV} reaches the maximum value of 13.3 kWh m^{-2} when $I_{threshold} = 100$ W m^{-2} in the E–W oriented greenhouse. The E_{PV} value of the N–S greenhouse is slightly greater than that of the E–W greenhouse. Actually, the N–S greenhouse PV blinds at $\theta = 90^\circ$ receive more direct sunlight impinging from a low elevation angle of the sun than those at $\theta = 0^\circ$ during early morning and late afternoon. This effect increases E_{PV} in $I_{threshold}$ of 100–400 W m^{-2} under the cloudless sky condition. Nevertheless, E_{PV} decreases monotonously with the increase of $I_{threshold}$ under actual sky conditions because the increased duration at $\theta = 90^\circ$ by frequent cloud covers diminishes E_{PV}. The $E_{surplus}$ values were ranged 8.1–13.4 kWh m^{-2} for the N–S greenhouse and 7.6–12.9 kWh m^{-2} for the E–W greenhouse.

In the actual sky estimation, μI_Hs were compared with $I_{threshold}$ to determine the times of PV blind turns. The PV blinds turn thousands of times when $I_{threshold}$ is set between 100 and 900 W m^{-2} because of the frequent partial cloud cover. The PV blinds rotate annually 16,984 times at most when $I_{threshold}$ is set at 400 W m^{-2}. In such a case, 0.16 kWh m^{-2} of electrical energy is used for the DC motor operation. The system's electrical energy consumption ($E_{motor} + E_{circuit} + E_{loss}$) accounts for about 3% of E_{PV}. The calculated E_{PV} in the N–S greenhouse is slightly greater than that in the E–W greenhouse. The E_{PV} value decreases as $I_{threshold}$ increases, irrespective of the greenhouse orientation. However, considering the energy consumption of the DC motors and the motor control circuits, $E_{surplus}$ reaches the maximum values of 7.5 and 7.4 kWh m^{-2}, respectively, in the N–S and E–W greenhouses when $I_{threshold}$ is set at 100 W m^{-2}. In the N–S greenhouse, $E_{surplus}$ is 7.5–4.5 kWh m^{-2}. It is 7.4–4.1 kWh m^{-2} in the E–W greenhouse. The system can produce

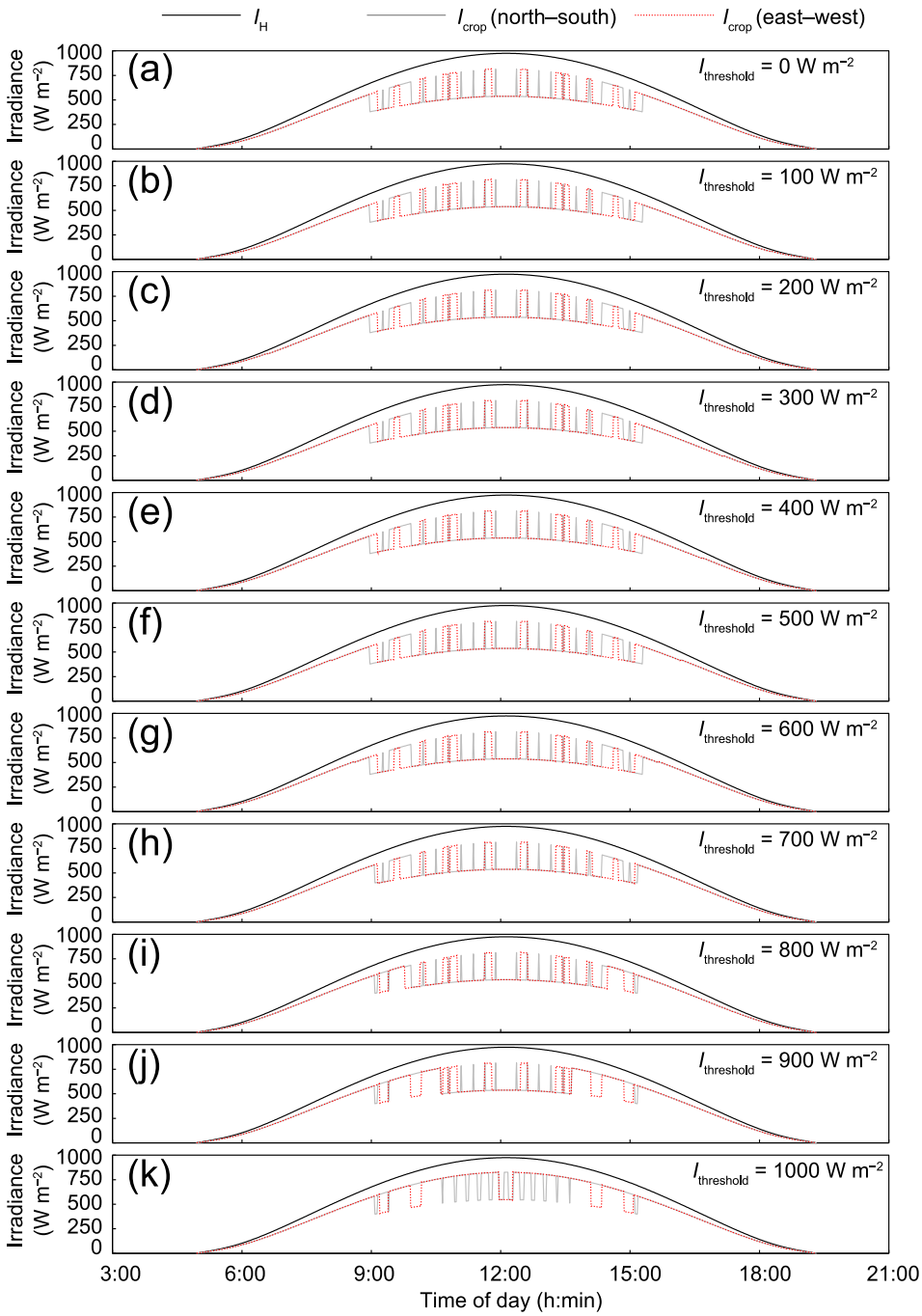

Fig. 12. Calculated I_H and I_{crop} on 15 June in the north–south and east–west oriented greenhouses when $I_{threshold}$ was set at 0–1,000 W m^{-2} with 100 W m^{-2} intervals.

average surplus electrical energy of at least 0.01 kWh m^{-2} day^{-1}. Assuming that 5 kWh m^{-2} yr^{-1} of surplus electrical energy is producible, the greenhouse owner's income from selling electricity is estimated as a function of the feed-in tariff and the operation duration (Fig. B.1). Twenty-year operation with a 0.2 € kWh^{-1} feed-in tariff yields a profit of 20 € m^{-2}. Accordingly, this price can be a target for PV blind system cost, including PV modules, an inverter, control circuits, and blind-framing metal structures. Unfortunately, our current system costs are much higher than this value, mostly because of its expensive custom-made PV modules.

In fact, the present PV blind system is intended to create a controlled sunlight condition in the greenhouse without commercial electricity input. Moreover, the PV blind produces surplus electrical energy to drive other fundamentally important devices used for greenhouse management (Fig. 4). The controlled greenhouse environment improves both crop quality and yield. For these reasons, the PV blind system described herein is particularly beneficial when operated as a stand-alone power system in remote regions where no power grids is available. Zhang et al. [53] reported that a low-cost seasonal solar soil heat storage system for greenhouse heating in Shanghai, China consumed 5.4 kWh m^{-2} yr^{-1} for auxiliary heating, pump, and electromagnetic valves. Another study described that keeping the temperature at 25 °C using a fan–pad cooling system for 300 m^2 greenhouse requires 4.5 kWh day^{-1} in Texcoco, Mexico [54]. McCartney and Lefsrud [55] reported that a cooling greenhouse with augmented natural ventilation in Trents, Barbados required 0.005 kWh m^{-2} day^{-1} of electrical energy input. Our shading

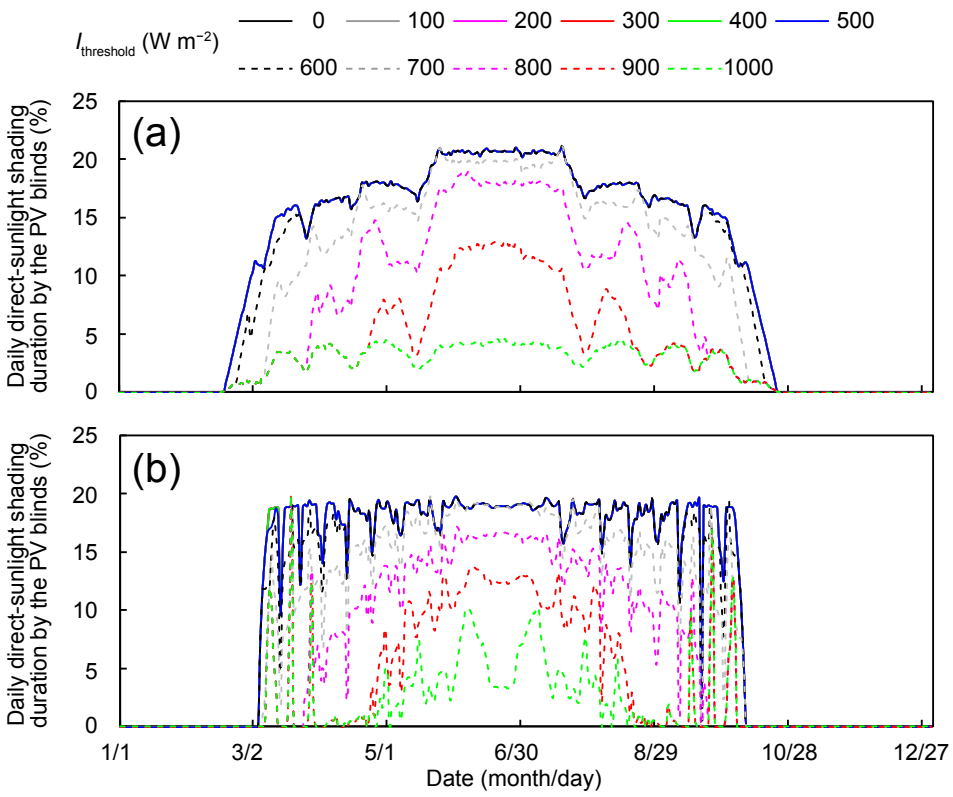

Fig. 13. Percentages of daily direct-sunlight shading durations by PV blinds in the north–south (a) and east–west (b) oriented greenhouses when $I_{threshold}$ was set at 0–1,000 W m^{-2} with 100 W m^{-2} intervals. It is noteworthy that lines of 100–400 W m^{-2} $I_{threshold}$s overlapped behind the $I_{threshold}$ = 500 W m^{-2} line.

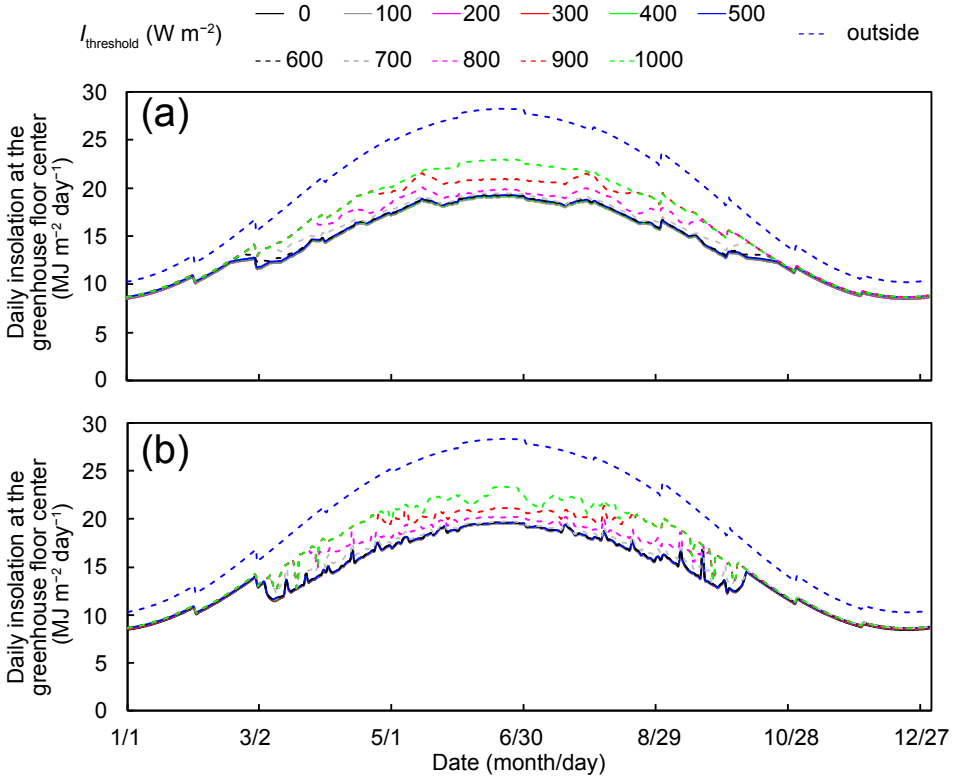

Fig. 14. Calculated daily insolation received at the center of the north–south (a) and east–west (b) oriented greenhouse. Daily insolation data outside the greenhouse are also presented.

system is useful when applied in combination with these energy-saving systems to compensate for the electricity demands of these greenhouses.

Solar irradiance (I_{crop}) received at the greenhouse floor center was calculated to estimate insolation received by crops. The 198 PV blinds and the sun paths can be projected onto an imaginary unit hemispherical surface with origin of O designated at the greenhouse floor center. Fig. 11 shows the projections of the PV blinds and sun paths on the hemisphere for the greenhouse orientations of N–S (Fig. 11a and b) and E–W (Fig. 11c and d). From point O, 76% and 95% of the sky area are visibly transparent when the respective θ values are 0° and 90°, based on the ratio of the 198 PV blind projection area to the hemispherical surface area. The sun paths of the 15th day of every month are also projected onto the hemispherical surface (Fig. 11). The PV blind shades the direct sunlight when their projections overlap. Assuming that the transmittances of the greenhouse glazing and the PV blind are 85% and 60%, respectively, the diffuse irradiance $I_{crop\ diffuse}$ (W m^{-2}) and direct irradiance $I_{crop\ direct}$ (W m^{-2}) irradiating onto the point O are calculated respectively as

$$I_{crop\ diffuse,t} = \begin{cases} I_{diffuse,t}\cdot 0.85\cdot 0.76 + I_{diffuse,t}\cdot 0.85\cdot 0.60\cdot(1-0.76) & (\theta = 0^\circ) \\ I_{diffuse,t}\cdot 0.85\cdot 0.95 + I_{diffuse,t}\cdot 0.85\cdot 0.60\cdot(1-0.95) & (\theta = 90^\circ) \end{cases} \quad (29)$$

and

$$I_{crop\ direct,t} = \begin{cases} I_{direct,t}\cdot 0.85\cdot 0.60 & \text{(projections overlap)} \\ I_{direct,t}\cdot 0.85 & \text{(projections not overlap)} \end{cases} \quad (30)$$

The global irradiance I_{crop} (W m^{-2}) received by crops at O is given as shown below:

$$I_{crop,t} = I_{crop\ direct,t} + I_{crop\ diffuse,t}. \quad (31)$$

Under the cloudless sky condition on 15 June I_H and I_{crop} in the N–S and E–W greenhouses (Fig. 12) with 100 W m^{-2} intervals of $I_{threshold}$ were calculated. The PV blinds retain $\theta = 0^\circ$ when the $I_{threshold}$ is set at 0 W m^{-2}. If $I_{threshold}$ is set as less than 600 W m^{-2}, diffuse irradiance increases slightly, whereas the direct irradiance is unchanged (Fig. 12a–g). In this case, the PV blinds shade the direct sunlight for 301 min in the N–S greenhouse and for 274 min in the E–W greenhouse. The shading durations are 287, 248, and 150 min when $I_{threshold}$ values are set respectively at 700, 800, and 900 W m^{-2} in the N–S greenhouse. In contrast, the shading durations are 274, 238, and 184 min when $I_{threshold}$ values are set respectively at 700, 800, and 900 W m^{-2} in the E–W greenhouse. The PV blinds retain their orientation at $\theta = 90^\circ$ throughout the day when the $I_{threshold}$ is set at 1,000 W m^{-2}. In this case, the direct sunlight is shaded by the PV blinds for 59 min in the N–S oriented greenhouse and 74 min in the E–W greenhouse.

The percentages of the daily direct-sunlight shading durations by the PV blinds in the N–S and E–W model greenhouses are presented in Fig. 13. Fig. 13a shows that the direct sunlight is not shaded by the PV blinds from 25 October through 15 February in the N–S oriented greenhouse. During this period, the sun paths viewed from O are below the greenhouse roof throughout the day. However, the unshaded period in the E–W greenhouse is from 9 October through 4 March (Fig. 13b), longer than that in the N–S greenhouse. When the $I_{threshold}$ is set below 500 W m^{-2} in the N–S greenhouse and below 400 W m^{-2} in the E–W greenhouse, the direct-sunlight shading durations are unchanged. In these cases, the PV blinds shade the direct-sunlight for about 959 hr per year in the N–S greenhouse and 939 hr per year in the E–W greenhouse. The longest direct-sunlight shading durations are 21.0% on 19 July in the N–S greenhouse and 19.7% on 1 June in the E–W greenhouse. When $I_{threshold}$ is set above 600 W m^{-2} in the N–S greenhouse and above 500 W m^{-2} in the E–W greenhouse, the direct-sunlight shading duration can be controlled properly by adjusting $I_{threshold}$.

Daily insolation J_{crop} (MJ m^{-2}) irradiating the greenhouse center O was calculated using equations (29), (30), and (31) when $I_{threshold}$ was set at 0–1,000 W m^{-2} with 100 W m^{-2} intervals under the cloudless sky condition (Fig. 14). Point O receives at most 23.0 MJ m^{-2} of insolation on 27 June in the N–S greenhouse and 23.3 MJ m^{-2} on 22 June in the E–W greenhouse when $I_{threshold}$ was set at 1,000 W m^{-2}. During winter, adjusting the $I_{threshold}$ value does not improve the light conditions in the greenhouse considerably because the PV blinds cannot shade the direct sunlight. By contrast, sunlight availability inside the greenhouse can be controlled effectively by adjusting the $I_{threshold}$ value during other seasons. For example, the average J_{crop} can be controlled to 19.0–22.9 MJ m^{-2} day^{-1} by adjusting the $I_{threshold}$ value from 0 to 1,000 W m^{-2} in the N–S greenhouse in June. Irrespective of the greenhouse orientation, a greater value of $I_{threshold}$s results in greater J_{crop}.

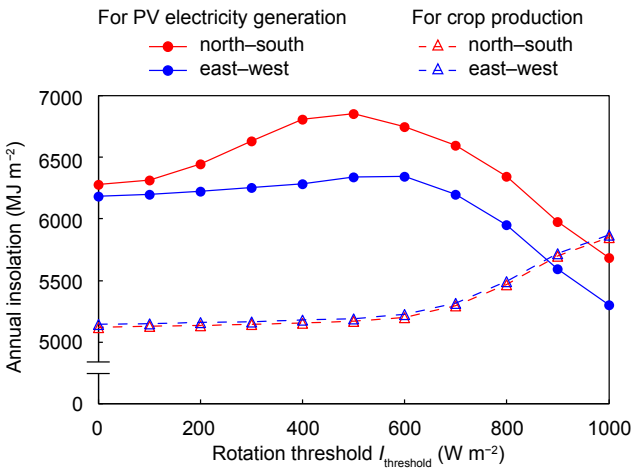

Fig. 15. Calculated annual insolation for PV electricity generation and crop production when the rotation threshold value changes at 100 W m^{-2} intervals from 0 to 1000 W m^{-2} in the model greenhouse under a cloudless sky condition.

Assuming that solar irradiance received on the greenhouse floor is distributed uniformly, then the annual insolation for crop production (J_{crop}) and PV electricity generation ($J_{front} + J_{back}$) can be calculated when $I_{threshold}$ was changed at 100 W m^{-2} intervals from 0 to 1,000 W m^{-2} (Fig. 15). Differences between J_{crop}s in the N–S and E–W greenhouses are small because the width and length of the model greenhouse are similar. By contrast, the estimated $J_{front} + J_{back}$ on the N–S greenhouse is greater than that on the E–W greenhouse. The maximum values of $J_{front} + J_{back}$ are 6,851 MJ m^{-2} when $I_{threshold} = 500$ W m^{-2} in the N–S greenhouse and 6,344 MJ m^{-2} when $I_{threshold} = 600$ W m^{-2} in the E–W greenhouse. At the maximum $J_{front} + J_{back}$s, the values of J_{crop} are, respectively, 75% and 82% of the maximum $J_{front} + J_{back}$s of the N–S and E–W greenhouses. The estimated annual J_{crop} crosses with $J_{front} + J_{back}$ when $I_{threshold} = 900$ W m^{-2} in the E–W greenhouse and 1,000 W m^{-2} on the N–S greenhouse. Results show that the same amount of insolation is useful for plant production and electricity generation at these intersections.

The annual values of J_{crop} are 5,124–5,852 MJ m^{-2} in the N–S greenhouse and 5,145–5,873 MJ m^{-2} in the E–W greenhouse under the cloudless sky condition (Fig. 15). These values correspond with average J_{crop} values of 14–16 MJ m^{-2} day^{-1} in both greenhouse orientations. Based on calculation presented in Section 4.4, clouds reduced J_H about 40%. Assuming that the J_{crop} value is also reduced 40%, 8–10 MJ m^{-2} day^{-1} of insolation is expected to irradiate crops in the greenhouse. Values of internal insolation below 5 MJ m^{-2} day^{-1} are reported as insufficient for the optimal growth of most greenhouse crops [30]. The optimal level commonly indicated for most horticultural crops is 6.0 MJ m^{-2} day^{-1} [13]. Japanese tomato cultivation reports have indicated that the greenhouse interior insolation was 10–15 MJ m^{-2} day^{-1} during spring–autumn [56,57]. Rosales et al. [58] reported cherry tomato fruit growth under 7 MJ m^{-2} day^{-1} of insolation. Mini tomato plants can be cultivated under conditions of less insolation. Perin et al. [59] reported the solar radiation threshold for two cultivars of mini tomato as 3.63 MJ

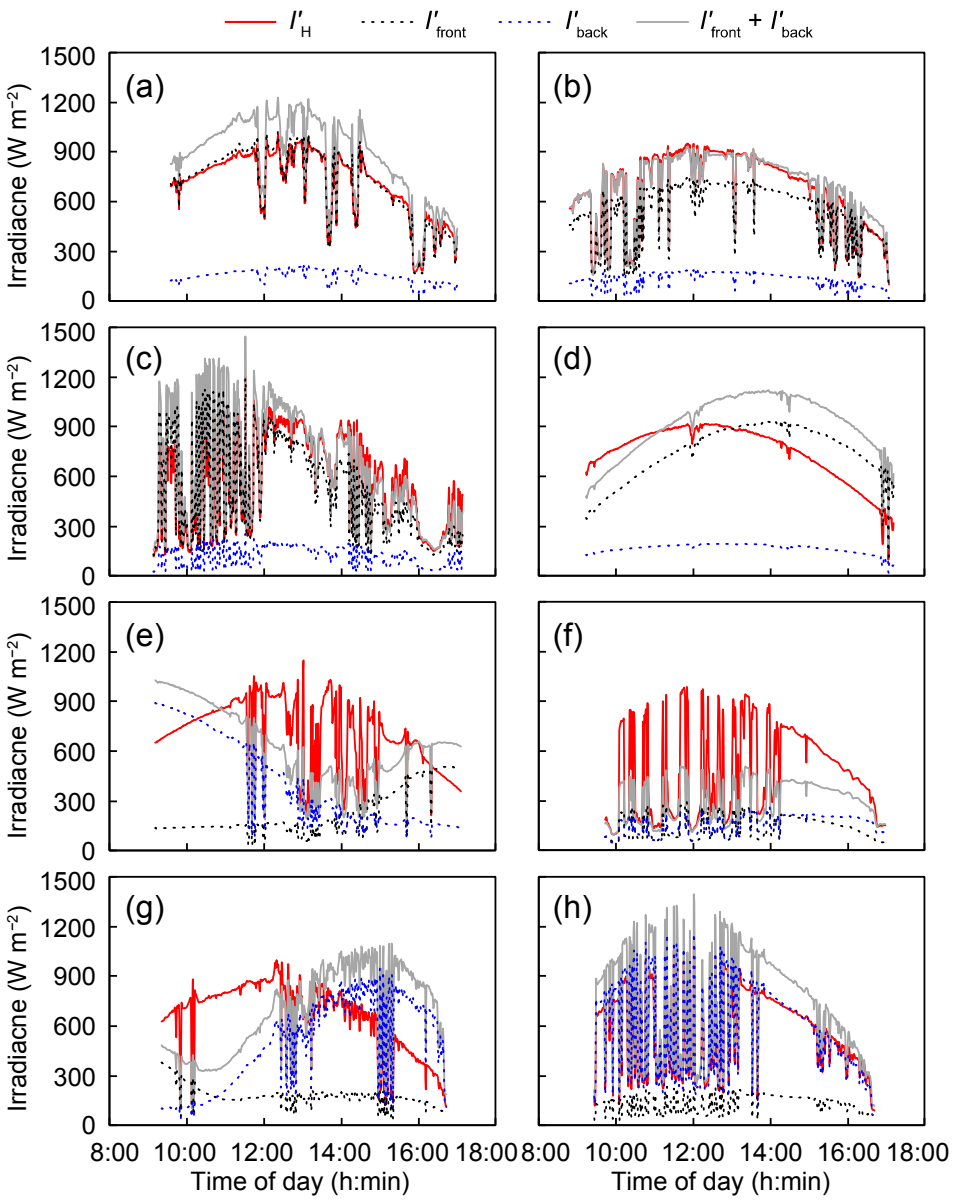

Fig. A1. Measured irradiances I'_H, I'_{front}, I'_{back}, and $I'_{front} + I'_{back}$, respectively, on 27 July (a), 31 July (b), 2 August (c), 3 August (d), 4 August (e), 8 September (f), 13 September (g), and 14 September (h) 2017.

m^{-2} day^{-1} inside the greenhouse. Other studies reports described daily insolation data for other crop species. For example, Aydinsakir et al. [60] cultivated lettuce under 0.6 to 4.1 MJ m^{-2} day^{-1} during winter and under insolation of 2.1–9.3 MJ m^{-2} day^{-1} during spring. In another study, leafy lettuce was cultivated under 6.6–20.9 MJ m^{-2} day^{-1} of insolation during spring and under 5.4–23.6 MJ m^{-2} day^{-1} during summer [61]. Lozano et al. [62] planted two cultivars of strawberry under 6.2–20.8 MJ m^{-2} day^{-1} of insolation. In addition, Gallardo et al. [63] reported that three cucumber crops were grown under 4–13 MJ m^{-2} day^{-1} of insolation in a greenhouse. Giménez et al. [64] planted four sweet pepper crops under 5.7–14.8 MJ m^{-2} day^{-1} of insolation. These reports suggest that the model greenhouse with a PV blind system is suitable for the solar radiation needs of major horticultural crops. In addition, as described in Fig. 14, adjusting the $I_{threshold}$ value to different light demands during the plant growth stage is beneficial. Using the present PV blind system, the balance of electrical energy generation and plant production can be regulated dynamically to improve the total utilization ratio of sunlight in the greenhouse.

5. Conclusions

Crop and photovoltaics (PV) coexistence represents a new and challenging effort for food and energy system transitions to more sustainable methods under the pressures of population growth and global climate change. Both crops and PVs need sunlight to achieve their essential energy conversion functions. Therefore, they compete for sunlight acquisition if they cover the same land area. This study investigated the feasibility of a greenhouse roof with an integrated semi-transparent PV-blind system to provide moderate shading conditions to greenhouse crops along with simultaneous electrical energy generation. The prototype PV-blind system was operated autonomously for one year in response to solar irradiance variation with surplus electrical energy generation. The electrical energy budget calculations of the PV blind system based on the energy balance equation indicated that 4–7 kWh m^{-2} yr^{-1} of surplus electrical energy are producible under actual sky conditions. Insolation available for greenhouse crops under the PV blind system was also calculated. By virtue of automatic blind operation, 8–10 MJ m^{-2} day^{-1} of average insolation, which is adequate for major

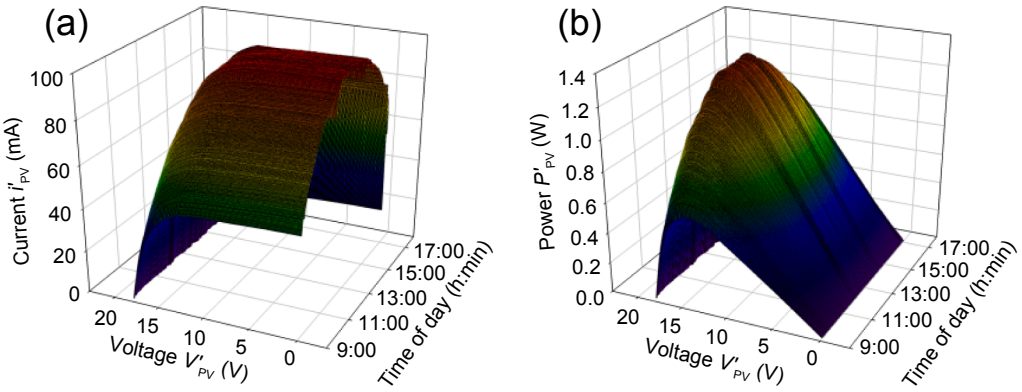

Fig. A2. Current–voltage (a) and power–voltage (b) characteristics of the single PV module measured on 3 August 2017.

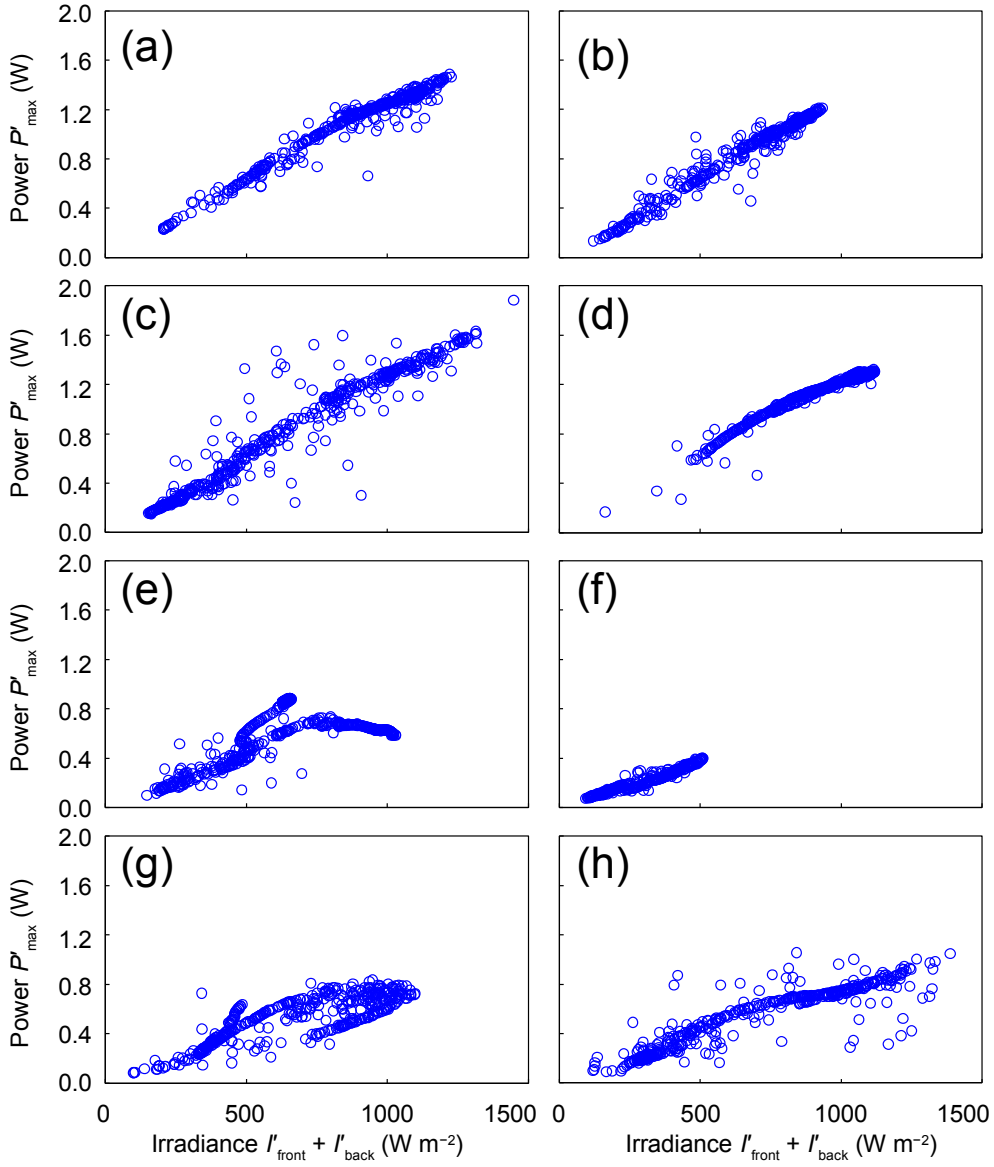

Fig. A3. Relation between the measured maximum output power of PV module P'_{max} and irradiances $I'_{front} + I'_{back}$ on 27 July (a), 31 July (b), 2 August (c), 3 August (d), 4 August (e), 8 September (f), 13 September (g), and 14 September (h) 2017.

Table A1
PV module orientation and inclination and the periods of the PV module electrical characteristic measurements.

Date	PV module front normal direction	PV module inclination angle β	Measurement period
27 Jul	South	26.5°	9:35–17:00
31 Jul	North		8:48–17:05
2 Aug	East		9:08–17:08
3 Aug	West		9:13–17:11
4 Aug	West	63.5°	9:10–17:06
8 Sep	South		9:43–16:59
13 Sep	East		9:20–16:43
14 Sep	North		9:25–16:41

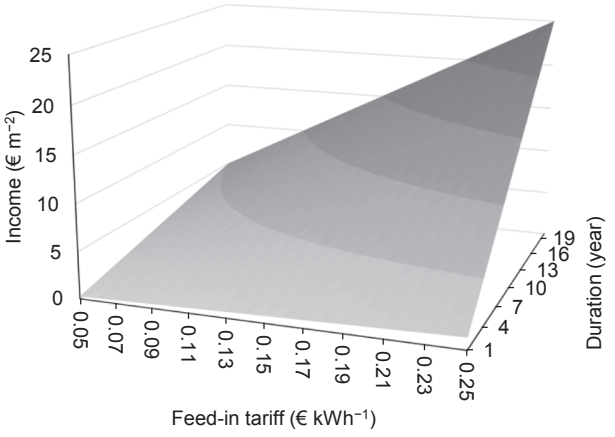

Fig. B1. Greenhouse owner's income from selling 5 kWh m^{-2} yr^{-1} of surplus electrical energy generated by the PV blind system to the grid, estimated as a function of the feed-in tariff and operation duration. For example, 20-year operation generates 100 kWh m^{-2}. If the feed-in tariff is set as 0.2 € kWh^{-1}, then the income would be 20 € m^{-2}.

greenhouse crop cultivation, are transmittable into the greenhouse under actual sky conditions. As demonstrated by the present model, growers can set the ratio of insolation apportionment to crop yield and electricity generation strategically.

CRediT authorship contribution statement

Zhi Li: Methodology, Software, Validation, Formal analysis, Investigation, Data curation, Writing - original draft, Visualization. **Akira Yano:** Conceptualization, Methodology, Investigation, Resources, Writing - review & editing, Supervision, Project administration, Funding acquisition. **Hidekazu Yoshioka:** Methodology, Software, Formal analysis, Writing - review & editing.

Declaration of Competing Interest

The authors declare that they have no known competing financial interests or personal relationships that could have appeared to influence the work reported in this paper.

Acknowledgments

This study was supported by JSPS KAKENHI (Grant Nos. (C) 15K07667 and (C)18K05903). The authors thank Sphelar Power Corporation (Kyoto, Japan) for fabricating the semi-transparent PV modules. We thank Profs. Makoto Ueno and Ichiro Kita of Shimane University and Yasuomi Ibaraki of Yamaguchi University for their support and encouragement.

Appendix A. PV module electrical characteristic measurements

The PV module was supported by a cubical framework 2 m above the ground (see Figs. A1–A3 and Table A1).

Appendix B. Estimation of the salable electricity generated by the PV blind system

See Fig. B1.

References

[1] Ntinas GK, Neumair M, Tsadilas CD, Meyer J. Carbon footprint and cumulative energy demand of greenhouse and open-field tomato cultivation systems under Southern and Central European climatic conditions. J Clean Prod 2017;142: 3617–26. https://doi.org/10.1016/j.jclepro.2016.10.106.
[2] Barron-Gafford GA, Pavao-Zuckerman MA, Minor RL, Sutter LF, Barnett-Moreno I, Blackett DT, et al. Agrivoltaics provide mutual benefits across the food–energy–water nexus in drylands. Nat Sustain 2019; 2: 848–855, 10.1038/s41893-019-0364-5.
[3] Dougka G, Briassoulis D. Load carrying capacity of greenhouse covering films under wind action: Optimising the supporting systems of greenhouse films. Biosys Eng 2020;192:199–214. https://doi.org/10.1016/j.biosystemseng.2020.01.020.
[4] Lamont WJ Jr. Overview of the use of high tunnels worldwide. HortTechnology 2009; 19: 25–29, 10.21273/HORTSCI.19.1.25.
[5] Dias GM, Ayer NW, Khosla S, Acker RV, Young SB, Whitney S, et al. Life cycle perspectives on the sustainability of Ontario greenhouse tomato production: Benchmarking and improvement opportunities. J Clean Prod 2017;140:831–9. https://doi.org/10.1016/j.jclepro.2016.06.039.
[6] Bambara J, Athienitis AK. Energy and economic analysis for the design of greenhouses with semi-transparent photovoltaic cladding. Renew Energy 2019; 131:1274–87. https://doi.org/10.1016/j.renene.2018.08.020.
[7] Ntinas GK, Dannehl D, Schuch I, Rocksch T, Schmidt U. Sustainable greenhouse production with minimised carbon footprint by energy export. Biosys Eng 2020; 189:164–78. https://doi.org/10.1016/j.biosystemseng.2019.11.012.
[8] Iwasaki Y, Aizawa M, Yoshida C, Takaichi M. Developing a new energy-saving, photosynthesis-promoting environmental control system for greenhouse production based on a heat pump with a heat storage system. J Agric Meteorol 2013;69:81–92. https://doi.org/10.2480/agrmet.69.2.4.
[9] The German Solar Energy Society. Planning and installing solar thermal systems: a guide for installers, architects, and engineers. James & James, London (UK); 2005.
[10] Hernandez RR, Armstrong A, Burney J, Ryan G, Moore-O'Leary K, Diédhiou I, et al. Techno–ecological synergies of solar energy for global sustainability. Nat Sustain 2019; 2: pp. 560–568, 10.1038/s41893-019-0309-z.
[11] Kozai T, He D, Ohtsuka H, Kamiya I. Simulation of solar radiation transmission into a lean-to greenhouse with photovoltaic cells on the roof —case study for a greenhouse with infinite longitudinal length. Environ Cont Biol 1999;37(2):101–8. https://doi.org/10.2525/ecb1963.37.101.
[12] Abdel-Ghany AM, Picuno P, Al-Helal I, Alsadon A, Ibrahim A, Shady M. Radiometric characterization, solar and thermal radiation in a greenhouse as affected by shading configuration in an arid climate. Energies 2015;8:13928–37. https://doi.org/10.3390/en81212404.
[13] Cossu M, Murgia L, Ledda L, Deligios PA, Sirigu A, Chessa F, et al. Solar radiation distribution inside a greenhouse with south-oriented photovoltaic roofs and effects on crop productivity. Appl Energy 2014;133:89–100. https://doi.org/10.1016/j.apenergy.2014.07.070.
[14] Cossu M, Yano A, Murgia L, Ledda L, Deligios PA, Sirigu A, et al. Effects of the photovoltaic roofs on the greenhouse microclimate. Acta Hortic 1170 (2017) 461–468, 10.17660/ActaHortic.2017.1170.57.
[15] Castellano S, Santamaria P, Serio F. Solar radiation distribution inside a monospan greenhouse with the roof entirely covered by photovoltaic panels. J Agric Eng, XLVII 2016;485. https://doi.org/10.4081/jae.2016.485.
[16] Marucci A, Cappuccini A. Dynamic photovoltaic greenhouse: Energy efficiency in clear sky conditions. Appl Energy 2016;170:362–76. https://doi.org/10.1016/j.apenergy.2016.02.138.
[17] López-Díaz G, Carreño-Ortega A, Fatnassi H, Poncet C, Díaz-Pérez M. The effect of different levels of shading in a photovoltaic greenhouse with a north–south orientation. Appl Sci 2020;10:882. https://doi.org/10.3390/app10030882.
[18] Buttaro D, Renna M, Gerardi C, Blando F, Santamaria P, Serio F. Soilless production of wild rocket as affected by greenhouse coverage with photovoltaic modules. Acta Sci Pol Hortorum Cultus 2016;15(2):129–42.
[19] Blando F, Gerardi C, Renna M, Castellano S, Serio F. Characterisation of bioactive compounds in berries from plants grown under innovative photovoltaic greenhouses. J Berry Res 2018;8:55–69. https://doi.org/10.3233/JBR-170258.
[20] Ureña-Sánchez R, Callejón-Ferre ÁJ, Pérez-Alonso J, Carreño-Ortega Á. Greenhouse tomato production with electricity generation by roof-mounted flexible solar panels. Sci Agric 2012;69:233–9. https://doi.org/10.1590/S0103-90162012000400001.

[21] Ezzaeri K, Fatnassi H, Bouharroud R, Gourdo L, Bazgaou A, Wifaya A, et al. The effect of photovoltaic panels on the microclimate and on the tomato production under photovoltaic canarian reenhouses. Sol Energy 2018;173:1126–34. https://doi.org/10.1016/j.solener.2018.08.043.
[22] Aroca-Delgado R, Pérez-Alonso J, Callejón-Ferre Á-J, Díaz-Pérez M. Morphology, yield and quality of greenhouse tomato cultivation with flexible photovoltaic rooftop panels (Almería-Spain). Sci Hortic 2019;257:108768. https://doi.org/10.1016/j.scienta.2019.108768.
[23] Bulgari R, Cola G, Ferrante A, Franzoni G, Mariani L, Martinetti L. Micrometeorological environment in traditional and photovoltaic greenhouses and effects on growth and quality of tomato (*Solanum lycopersicum* L.). Ital J Agrometeorol 2015;2:27–38.
[24] Kavga A, Strati IF, Sinanoglou VJ, Fotakis C, Sotiroudis G, Christodoulou P, et al. Evaluating the experimental cultivation of peppers in low-energy-demand greenhouses. An interdisciplinary study. J Sci Food Agric 2019;99:781–9. https://doi.org/10.1002/jsfa.9246.
[25] Tang Y, Ma X, Li M, Wang Y. The effect of temperature and light on strawberry production in a solar greenhouse. Sol Energy 2020;195:318–28. https://doi.org/10.1016/j.solener.2019.11.070.
[26] Vadiee A, Martin V. Solar blind system- solar energy utilization and climate mitigation in glassed buildings. Energy Procedia 2014;57:2023–32. https://doi.org/10.1016/j.egypro.2014.10.067.
[27] Vadiee A, Yaghoubi M, Martin V, Bazargan-Lari Y. Energy analysis of solar blind system concept using energy system modelling. Sol Energy 2016;139:297–308. https://doi.org/10.1016/j.solener.2016.09.039.
[28] Alinejad T, Yaghoubi M, Vadiee A. Thermo-environomic assessment of an integrated greenhouse with an adjustable solar photovoltaic blind system. Renew Energy 2020;156:1–13. https://doi.org/10.1016/j.renene.2020.04.070.
[29] Marucci A, Cappuccini A. Dynamic photovoltaic greenhouse: Energy balance in completely clear sky condition during the hot period. Energy 2016;102:302–12. https://doi.org/10.1016/j.energy.2016.02.053.
[30] Moretti S, Marucci A. A photovoltaic greenhouse with variable shading for the optimization of agricultural and energy production. Energies 2019;12:2589. https://doi.org/10.3390/en12132589.
[31] Moretti S, Marucci A. A photovoltaic greenhouse with passive variation in shading by fixed horizontal PV panels. Energies 2019;12:3269. https://doi.org/10.3390/en12173269.
[32] Li Z, Yano A, Cossu M, Yoshioka H, Kita I, Ibaraki Y. Electrical energy producing greenhouse shading system with a semi-transparent photovoltaic blind based on micro-spherical solar cells. Energies 2018;11:1681. https://doi.org/10.3390/en11071681.
[33] Li Z, Yano A, Cossu M, Yoshioka H, Kita I, Ibaraki Y. Shading and electric performance of a prototype greenhouse blind system based on semi-transparent photovoltaic technology. J Agric Meteorol 2018;74:114–22. https://doi.org/10.2480/agrmet.D-17-00047.
[34] Gao Y, Dong J, Isabella O, Santbergen R, Tan H, Zeman M, et al. Modeling and analyses of energy performances of photovoltaic greenhouses with sun-tracking functionality. Appl Energy 2019;233–234:424–42. https://doi.org/10.1016/j.apenergy.2018.10.019.
[35] Yoshioka H, Li Z, Yano A. An optimal switching approach toward cost-effective control of a stand-alone photovoltaic panel system under stochastic environment. Appl Stoch Models Bus Ind 2019;35:1366–89. https://doi.org/10.1002/asmb.2485.
[36] Hassanien RHE, Li M, Lin WD. Advanced applications of solar energy in agricultural greenhouses. Renew Sust Energ Rev 2016;54:989–1001. https://doi.org/10.1016/j.rser.2015.10.095.
[37] Yano A, Cossu M. Energy sustainable greenhouse crop cultivation using photovoltaic technologies. Renew Sust Energ Rev 2019;109:116–37. https://doi.org/10.1016/j.rser.2019.04.026.
[38] Marucci A, Zambon I, Colantoni A, Monarca D. A combination of agricultural and energy purposes: Evaluation of a prototype of photovoltaic greenhouse tunnel. Renew Sust Energ Rev 2018;82:1178–86. https://doi.org/10.1016/j.rser.2017.09.029.
[39] Cossu M, Cossu A, Deligios PA, Ledda L, Li Z, Fatnassi H, et al. Assessment and comparison of the solar radiation distribution inside the main commercial photovoltaic greenhouse types in Europe. Renew Sust Energ Rev 2018;94:822–34. https://doi.org/10.1016/j.rser.2018.06.001.
[40] Cossu M, Yano A, Solinas S, Deligios PA, Tiloca MT, Cossu A, et al. Agricultural sustainability estimation of the European photovoltaic greenhouses. Eur J Agron 2020;118:126074. https://doi.org/10.1016/j.eja.2020.126074.
[41] Sun Y, Shanks K, Baig H, Zhang W, Hao X, Li Y, et al. Integrated semi-transparent cadmium telluride photovoltaic glazing into windows: Energy and daylight performance for different architecture designs. Appl Energy 2018;231:972–84. https://doi.org/10.1016/j.apenergy.2018.09.133.
[42] Peng J, Curcija DC, Thanachareonkit A, Lee ES, Goudey H, Selkowitz SE. Study on the overall energy performance of a novel c-Si based semitransparent solar photovoltaic window. Appl Energy 2019;242:854–72. https://doi.org/10.1016/j.apenergy.2019.03.107.
[43] Gao Y, Dong J, Isabella O, Santbergen R, Tan H, Zeman M, et al. A photovoltaic window with sun-tracking shading elements towards maximum power generation and non-glare daylighting. Appl Energy 2018;228:1454–72. https://doi.org/10.1016/j.apenergy.2018.07.015.
[44] Luo Y, Zhang L, Liu Z, Su X, Lian J, Luo Y. Coupled thermal-electrical-optical analysis of a photovoltaic-blind integrated glazing façade. Appl Energy 2018;228:1870–86. https://doi.org/10.1016/j.apenergy.2018.07.052.
[45] Markvart T. Solar Electricity. 2nd ed. Chichester (UK): John Wiley & Sons; 2000.
[46] Page J. The role of solar radiation climatology in the design of photovoltaic systems. In: Practical Handbook of Photovoltaics: Fundamentals and Applications. Elsevier, Oxford (UK); 2003, pp. 5–66.
[47] Yano A, Furue A, Kadowaki M, Tanaka T, Hiraki E, Miyamoto M, et al. Electrical energy generated by photovoltaic modules mounted inside the roof of a north–south oriented greenhouse. Biosys Eng 2009;103:228–38. https://doi.org/10.1016/j.biosystemseng.2009.02.020.
[48] Tanaka K, Kosugi Y, Nakamura A. Impact of leaf physiological characteristics on seasonal variation in CO_2, latent and sensible heat exchanges over a tree plantation. Agric For Meteorol 2002;114:103–22. https://doi.org/10.1016/S0168-1923(02)00128-4.
[49] Kosugi Y, Takanashi S, Matsuo N, Tanaka K, Tanaka H. Impact of leaf physiology on gas exchange in a Japanese evergreen broad-leaved forest. Agric For Meteorol 2006;139:182–99. https://doi.org/10.1016/j.agrformet.2006.06.009.
[50] National Astronomical Observatory of Japan. Chronological Scientific Tables 2007 [in Japanese], Maruzen Publishing, Tokyo (Japan) (2006), pp. 244.
[51] Cossu M, Yano A, Li Z, Onoe M, Nakamura H, Matsumoto T, et al. Advances on the semi-transparent modules based on micro solar cells: First integration in a greenhouse system. Appl Energy 2016;162:1042–51. https://doi.org/10.1016/j.apenergy.2015.11.002.
[52] Butcher JC. Numerical methods for ordinary differential equations in the 20th century. J Comput Appl Math 2000;125:1–29. https://doi.org/10.1016/S0377-0427(00)00455-6.
[53] Zhang L, Xu P, Mao J, Tang X, Li Z, Shi J. A low cost seasonal solar soil heat storage system for greenhouse heating: Design and pilot study. Appl Energy 2015;156:213–22. https://doi.org/10.1016/j.apenergy.2015.07.036.
[54] Romantchik E, Ríos E, Sánchez E, López I, Sánchez JR. Determination of energy to be supplied by photovoltaic systems for fan-pad systems in cooling process of greenhouses. Appl Therm Eng 2017;114:1161–8. https://doi.org/10.1016/j.applthermaleng.2016.10.011.
[55] McCartney L, Lefsrud MG. Field trials of the Natural Ventilation Augmented Cooling (NVAC) greenhouse. Biosys Eng 2018;174:159–72. https://doi.org/10.1016/j.biosystemseng.2018.07.004.
[56] Kinoshita T, Yamazaki H, Inamoto K, Yamazaki H. Analysis of yield components and dry matter production in a simplified soilless tomato culture system by using controlled-release fertilizers during summer–winter greenhouse production. Sci Hortic 2016;202:17–24. https://doi.org/10.1016/j.scienta.2016.02.019.
[57] Kinoshita T, Yamazaki H, Inamoto K. Effects of interplanting on fruit yield and dry matter production in greenhouse-grown tomato by integrating two different crop periods. Jarq - Jap Agricl Res Q 2019;53:295–304. https://doi.org/10.6090/jarq.53.295.
[58] Rosales MA, Rubio-Wilhelmi MM, Castellano R, Castilla N, Ruiz JM, Romero L. Sucrolytic activities in cherry tomato fruits in relation to temperature and solar radiation. Sci Hortic 2007;113:244–9. https://doi.org/10.1016/j.scienta.2007.03.015.
[59] Perin L, Peil RMN, Trentin R, Streck EA, DaRosa DSB, Hohn D, et al. Solar radiation threshold and growth of mini tomato plants in mild autumn/winter condition. Sci Hortic 2018;239:156–62. https://doi.org/10.1016/j.scienta.2018.05.037.
[60] Aydinsakir K, Karaca C, Ozkan CF, Dinc N, Buyuktas D, Isik M. Excess nitrogen exceeds the European standards in lettuce grown under greenhouse conditions. Agron J 2019;111:764–9. https://doi.org/10.2134/agronj2018.07.0425.
[61] Fallovo C, Rouphael Y, Cardarelli M, Rea E, Battistelli A, Colla G. Yield and quality of leafy lettuce in response to nutrient solution composition and growing season. J Food Agric Environ 2009;7(2):456–62. https://doi.org/10.1234/4.2009.1695.
[62] Lozano D, Ruiz N, Gavilán P. Consumptive water use and irrigation performance of strawberries. Agric Water Manage 2016;169:44–51. https://doi.org/10.1016/j.agwat.2016.02.011.
[63] Gallardo M, Padilla FM, Peña-Fleitas MT, de Souza R, Rodríguez A, Thompson RB. Crop response of greenhouse soil-grown cucumber to total available N in a Nitrate Vulnerable Zone. Eur J Agron 2020;114:125993. https://doi.org/10.1016/j.eja.2019.125993.
[64] Giménez C, Gallardo M, Martínez-Gaitán C, Stöckle CO, Thompson RB, Granados MR. VegSyst, a simulation model of daily crop growth, nitrogen uptake and evapotranspiration for pepper crops for use in an on-farm decision support system. Irrig Sci 2013;31:465–77. https://doi.org/10.1007/s00271-011-0312-2.